SYNTHESIS OF SnO_2 AND SnS_2 NANOMATERIALS BY CO-PRECIPITATION AND HYDROTHERMAL METHOD

A Thesis Submitted

In Partial Fulfillment of the Requirements for the

Degree of

MASTERS OF SCIENCE

in

Physics

by

LOVELY SEHRAWAT

(24/MSCPHY/36)

Under the supervision of

PROF. VINOD SINGH

Department of Applied Physics

DELHI TECHNOLOGICAL UNIVERSITY

(Formerly Delhi College of Engineering)

Shahbad Daulatpur, Main Bawana road, Delhi – 110042

CANDIDATE'S DECLARATION

I **LOVELY SEHRAWAT** hereby certify that the work which is presented in this thesis entitled **"SYNTHESIS OF SnO_2 AND SnS_2 NANOMATERIALS BY CO-PRECIPITATION AND HYDROTHERMAL METHOD",** in partial fulfillment of the requirements for the award of the Degree of Masters of Science in Physics, submitted in the Department of Applied Physics, Delhi Technological University is an authentic record of my own work carried out during the period from July, 2025 to May 2026 under the supervision of Prof. Vinod Singh.

The matter presented in the thesis has not been submitted by me for the award of any other degree of this or any other Institute.

Candidate's Signature

CERTIFICATE

Certified that **Lovely Sehrawat** (24/MSCPHY/36) has carried out their search work presented in this thesis entitled **"SYNTHESIS OF SnO_2 AND SnS_2 NANOMATERIALS BY CO-PRECIPITATION AND HYDROTHERMAL METHOD"** for the award of **Master of Science** from the Department of Applied Physics, Delhi Technological University, Delhi, under my supervision. The thesis embodies results of original work, and studies are carried out by the student herself, and the contents of the thesis do not form the basis for the award of any other degree to the candidate or to anybody else from this or any other University.

Signature
Prof. Vinod Singh
(Head of Department)
Delhi Technological University, Delhi-110042

Date: 29/May/2026

PLAGIARISM VERIFICATION

Title of the Thesis: SYNTHESIS OF SnO_2 AND SnS_2 NANOMATERIALS BY CO-PRECIPITATION AND HYDROTHERMAL METHOD Total Pages: Name of the Scholar: Lovely Sehrawat

Supervisor

Prof. Vinod Singh

Department of Applied Physics

This is to report that the above thesis was scanned for similarity detection. Process and outcome are given below:

Software used: _____ Similarity Index: _____, Total Word Count: _____

Date: _____

Candidate's Signature **Signature of Supervisor**

ABSTRACT

SnO_2 and SnS_2 nanomaterials were synthesized via co-precipitation and hydrothermal methods. The resulting samples were characterized using XRD, FESEM, Ultraviolet-Visible (UV-Vis) absorption spectroscopy, and FTIR. XRD analysis showed that both synthesis methods produced pure phases of SnO_2 and SnS_2. For SnO_2, the hydrothermally synthesized material showed sharper and more intense peaks compared to the co-precipitation method, indicating better crystallinity. Similarly, SnS_2 synthesized by the hydrothermal method showed well-defined, sharp, and intense peaks, which confirms the improved crystallinity. FESEM analysis revealed a strong dependence of morphology on the synthesis technique. Elemental composition and purity of the SnO_2 and SnS_2 nanomaterials were determined using EDX. Researchers used UV-Vis spectroscopy for studying optical characteristics of synthesized SnO_2 and SnS_2 nanomaterials. FTIR analysis confirmed the presence of Sn-O and Sn-S bonds, along with other functional groups. Overall, the results show that the synthesis method and material structure together influence the structural, morphological, and optical properties of the prepared nanomaterials.

KEYWORDS: SnO_2, SnS_2, Co-precipitation synthesis, Hydrothermal synthesis, XRD, UV-Vis spectroscopy, FTIR, EDX.

ACKNOWLEDGEMENT

I would like to express my sincere gratitude to my supervisor, Professor Vinod Singh, Head of the Department of Applied Physics, Delhi Technological University, for his valuable guidance, constant encouragement, and support throughout the completion of this thesis. His knowledge, motivation, and insightful suggestions greatly helped me during my research work.

I am also deeply thankful to Dr M. S. Mehta for providing me the opportunity to carry out FTIR characterization in his laboratory. I would like to extend my heartfelt thanks to Renuka Bokolia, ma'am, for allowing me to perform UV-Visible spectroscopy in her laboratory and for her kind assistance and cooperation.

A special note of appreciation goes to my PhD scholars and mentors, Jasveer Singh and Bharat Bhushan, whose guidance, patience, and continuous support helped me at every stage of this work. Their suggestions and encouragement made this research journey much smoother and more enriching.

I am also grateful to all the laboratory members for their help, friendly environment, and cooperation during my research work.

Finally, I would like to thank my family and friends for their unconditional support, understanding, motivation, and encouragement throughout my academic journey. Their belief in me has always been a source of strength and inspiration.

LOVELY SEHRAWAT

CONTENTS

LIST OF FIGURES

Fig. 3.13 FTIR of SnS_2 synthesized by the (a) Hydrothermal and (b) Co-precipitation method.

Fig. 3.14 UV-Vis spectra of (a) SnO_2 by co-precipitation method, (b) SnO_2 by hydrothermal method, (c) SnS_2 by co-precipitation method and (d) SnS_2 by hydrothermal method.

LIST OF SYMBOLS AND ABBREVIATIONS

3-D	**Three Dimensional**
DI water	**Distilled water**
XRD	**X-Ray Diffraction**
FWHM	**Full Width at Half Maximum**
W-H PLOT	**Williamson Hall plot**
FESEM	**Field Emission Scanning Electron Microscope**
FTIR	**Fourier Transform Infrared spectroscopy**
EDAX	**Energy Dispersive X-Ray Analysis**

CHAPTER -1

INTRODUCTION

1.1 Nanomaterials

Nanomaterials are the basis of nanoscience and nanotechnology. Nanostructure science and technology is a wide multidisciplinary area of study and development that has seen rapid growth around the world in recent years. Materials with at least one dimension smaller than approximately 100 nanometers are referred to as nanomaterials. A nanometre is one-millionth of a millimetre - a human hair is about 100,000 times the size of a nanometre. Nanomaterials are interesting due to unique optical, magnetic, electrical and other properties that occur at this size. These emergent features could significantly impact electronics, medicine, and other industries [1]. At the nanoscale, nanostructures can have 1D, 2D, or 3D dimensions. Nanomaterials are categorized according to their dimensions as follows:

- **0-D nanostructures**, such as spheres and clusters.
- **1-D nanostructures**, such as films, coatings, and multilayers.
- **2-D nanostructures**, such as tubes, fibers, wires, and platelets.
- **3-D nanostructures**, such as particles, quantum dots, and hollow spheres [2].

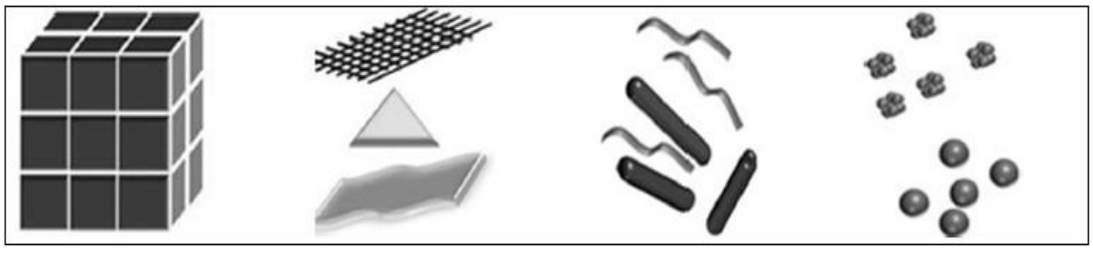

Fig. 1.1 Types of nanomaterials: a) 0D, b) 1D, c) 2D, d) 3D Nanomaterials (Source: Fehim Findik, Nanomaterials and Their Applications) [3]

Nanomaterials are categorized into various types based on their morphology, size, properties, and constituent components. These include carbon-based, metal, semiconductor, polymeric, and lipid-based nanomaterials [3]. Nanomaterials have found widespread applications in various fields due to their unique physicochemical properties. In the construction industry, they are used to improve the mechanical strength and durability of materials through advanced nanocomposites and coatings. In the field of medicine, nanomaterials play a crucial role in drug delivery, diagnostics, and biomedical devices. They are also applied in agriculture to enhance the efficiency of fertilizers and pesticides [4]. Furthermore, nanomaterials are extensively used in environmental applications such as water purification and pollution control, as well as in energy-related technologies, including solar cells, batteries, and catalysis [5].

Classification of Nanomaterials by Composition

They can also be classified according to the composition and structure of the materials. The physical, chemical, electrical, optical and mechanical properties of the nanomaterials depend on the material they are made of. The major categories are carbon-based, metal-based, metal oxide-based, polymer-based and composite-based nanomaterials.

1. Carbon-Based Nanomaterials:

Carbon-based nanomaterials are made entirely of carbon atoms in an ordered structure at the nanoscale. These nanomaterials are widely studied for their mechanical strength, electrical conductivity, high thermal stability, and high surface area to volume ratio. There are several allotropes of carbon existing at the nanoscale, such as fullerenes, carbon nanotubes, graphene, and carbon quantum dots.

Fullerenes: These are spherical and cage-like molecules composed only of carbon atoms with an arrangement in the form of hexagonal and pentagonal rings. The most common Fullerene is the C molecule and is called the Buckyball. These are considered to have special optical and electrical properties and are widely investigated for photovoltaic and medical applications, as drug delivery systems and bio-imaging.

Carbon Nanotubes: These are cylindrical molecules formed by the roll-up of single or multiple layers of graphite. Carbon nanotubes can be classified further into single-walled (SWCNTs) and multi-walled carbon nanotubes (MWCNTs). They possess unique properties such as strength, high electrical conductivity and flexibility, making them ideal for nanoelectronics, sensors and reinforced composites as well as energy storage.

Graphene: Graphene is a 2D material made up of only carbon atoms arranged in a honeycomb structure with high electrical and thermal conductivity, strength and the lowest weight among materials known. It has applications in smart electronics, supercapacitors, transparent conductive layers and biosensors.

Carbon Quantum Dots: These are tiny nano carbon particles that produce strong fluorescent light when excited and also have unique chemical and biological properties with excellent stability and bio-compatibility, useful in bio-imaging, biosensing, light-emitting devices, and photocatalysis.

2. Metal-Based Nanomaterials:

These are composed of pure metallic nanoparticles such as Au, Ag, Pt and Pd. Nanoparticles of metals display specific properties that are different from their bulky counterparts. These specific properties at the nanoscale include optics, catalytic and magnetic properties and electronic effects which occur due to quantum confinement and high surface-area-to-volume ratio.

Gold nanoparticles: They are highly investigated due to their superb bio-compatibility, specific surface plasmon resonance properties, useful for drug delivery and imaging, and also used in sensing and cancer therapy. Their optical properties are easily tunable.

Silver nanoparticles: These nanoparticles have shown superior antibacterial and anti-fungal activity and therefore are widely used in medical coating applications, the textile industry, wound dressings, water purification and also in the packaging industries.

Platinum and Palladium Nanoparticles: Both of these nanomaterials are widely studied and used for their excellent catalytic properties. They are used in fuel cells, hydrogen storage, and chemical reactions.

3. Metal Oxide-Based Nanomaterials:

Metal oxides composed of metal and oxygen are semiconductors with unique magnetic and photocatalytic properties, which make them attractive for applications in environmental protection and industry.

Titanium Dioxide Nanoparticles: Used extensively for its photocatalytic property, these nanoparticles absorb ultraviolet rays, which is exploited in the production of sunscreens, self-cleaning surfaces, air and water purification systems. They effectively degrade organic compounds and harmful microorganisms.

Zinc Oxide Nanoparticles: This semiconductor exhibits strong antibacterial activity and UV-blocking properties and is used for sensors, smart optoelectronic devices and in medicine for a wide range of applications due to low toxicity and high chemical stability.

Iron Oxide Nanoparticles: These are magnetic nanomaterials and therefore are utilized in MRI's, for the delivery of drugs at targeted sites and also in magnetic storage media.

4. Polymer-Based Nanomaterials:

These nanomaterials are fabricated using naturally occurring or synthetic polymers. They are extremely important in biomaterial science as these materials are biocompatible and biodegradable.

The materials discussed include nanospheres, nanocapsules, dendrimers, and polymeric micelles. Nanospheres are solid particles in which the desired components are distributed within a polymer matrix whereas nanocapsules involve a polymeric coat surrounding the drug material. Dendrimers have a branched structure with a multitude of surface functionalities. Their important applications include controlled

delivery of drugs and gene therapy, wound healing, vaccine delivery, and the development of smart diagnostic and therapeutic devices.

5. Composite Nanomaterials:

A composite nanomaterial is formed by mixing two or more nanomaterials or by incorporating nanoparticles into the matrix of another nanomaterial. The addition of nanoscale materials results in improvement of mechanical, electrical, optical, thermal and chemical properties of the resulting material. They offer excellent strength, durability, corrosion resistance and also electrical conductivity, compared to their conventional counterparts. Composite nanomaterials can be polymer based, ceramic based or even metal-based. The applications of composite nanomaterials lie in aerospace and automotive fields, the sports equipment industry, food packaging, and advanced electronics.

Among all nanomaterials, metal oxide and metal sulfide nanoparticles are the most widely used due to their unique characteristics and broad range of applications.

Metal Oxide Nanomaterials

Among various nanomaterials, metal oxide nanomaterials are one of the widely studied ones due to their prominent optical, electrical, catalytic and thermal properties. These are characterized by their good chemical stability, large surface area and adjustable electronic properties on nanoscale dimensions. Their applications are found in gas sensors, photocatalysis, solar cells, batteries, the biomedical field and environmental cleanup. Out of several metal oxides, tin oxide is being explored extensively due to its high electron mobility, strong oxidation stability, large band gap and superior sensing performance. Applications are found in gas sensing, lithium-ion battery, photocatalysis, optoelectronics, and transparent conducting oxide electrodes.

Metal Sulfide Nanomaterials

Metal sulfide nanomaterials are a key class of semiconductor nanomaterials showing fascinating optical and electronic properties as they have a narrow band gap and strong absorption in the visible light region. Their research interest is developed in the field

of photocatalysis, solar cells, energy storage and sensors. Among metal sulfides, tin disulfide is an important layered semiconductor material that has shown great potential due to its good optical absorption, environmentally friendly nature, high surface area, and efficient charge-transport characteristics. Its applications are found in photocatalytic degradation, energy storage, photodetectors and gas sensors.

As far as the metal oxide nanomaterials are concerned, characteristics that give these nanophase materials vital importance in nanotechnology today are: their nonlinear optical properties vary from material to material, higher ductility at high temperature than coarse-grained ceramics, cold welding feature, superparamagnetic behaviour, and unique catalytic, sensitivity and selective activity [6]. Metal sulfide nanoparticles have come to the forefront owing to their photovoltaic and electrochemical properties, which show promise against metal oxide nanoparticles. While nanoparticles are widely utilised for their remarkable performance in diverse fields, including catalysis, sensors, electronics, cosmetics, and photovoltaic devices, there is room for further development [7].

1.2 SnO_2 nanomaterial

Tin(IV) oxide (Tin oxide or stannic oxide) is one of the well-known metal oxide semiconductors used for electronics, gas sensors, solar cells, photocatalysis and energy storage devices. Its chemical formula is SnO_2, in which the tin is at the +4 oxidation state and oxygen is at -2 oxidation state. Typically, it is a white crystalline solid and is known for its high chemical and thermal stability. The material is an n-type semiconductor due to intrinsic oxygen vacancies and tin interstitial defects, giving free electrons as charge carriers. It has a wide direct band gap of about 3.6 eV, and the film is transparent in the visible region, yet electrically conductive. Hence, this optically transparent and electrically conductive property is well explored in the application for transparent conducting electrodes and optoelectronic devices. It crystallizes in the tetragonal rutile crystal structure with space group P4/mnm. Each tin atom is octahedrally surrounded by six oxygen atoms, and each oxygen atom is tetrahedrally surrounded by three tin atoms. Rutile structure is also responsible for its superior mechanical strength and thermal stability.

Some of the key properties of SnO_2 are:

1. Wide band gap (approx. 3.6 eV), which makes the material optically transparent.

2. High electrical conductivity is achieved due to the existence of oxygen vacancies in the SnO_2 film.

3. Good thermal and chemical stability.

4. Sensitive to gases and hence used in gas sensors.

5. Good electron mobility and rapid charge transport.

6. High surface-to-volume ratio in the case of nanostructured SnO_2.

7. Environmentally friendly and non-toxic material.

8. Strong photocatalytic activity in UV light.

All these excellent properties of SnO_2 make it widely explored in the form of thin films or nanostructures for its applications in gas sensors, lithium-ion batteries, solar cells, supercapacitors and photocatalytic degradation of pollutants [8].

1.2.1 Synthesis methods of SnO_2

Several synthesis methods, including sol-gel, hydrothermal, co-precipitation, chemical vapour deposition, and microwave-assisted routes, have been applied to fabricate SnO_2 nanostructures. However, hydrothermal and co-precipitation routes are commonly chosen because of their simple, inexpensive, and controllable methods for shaping morphologies [9].

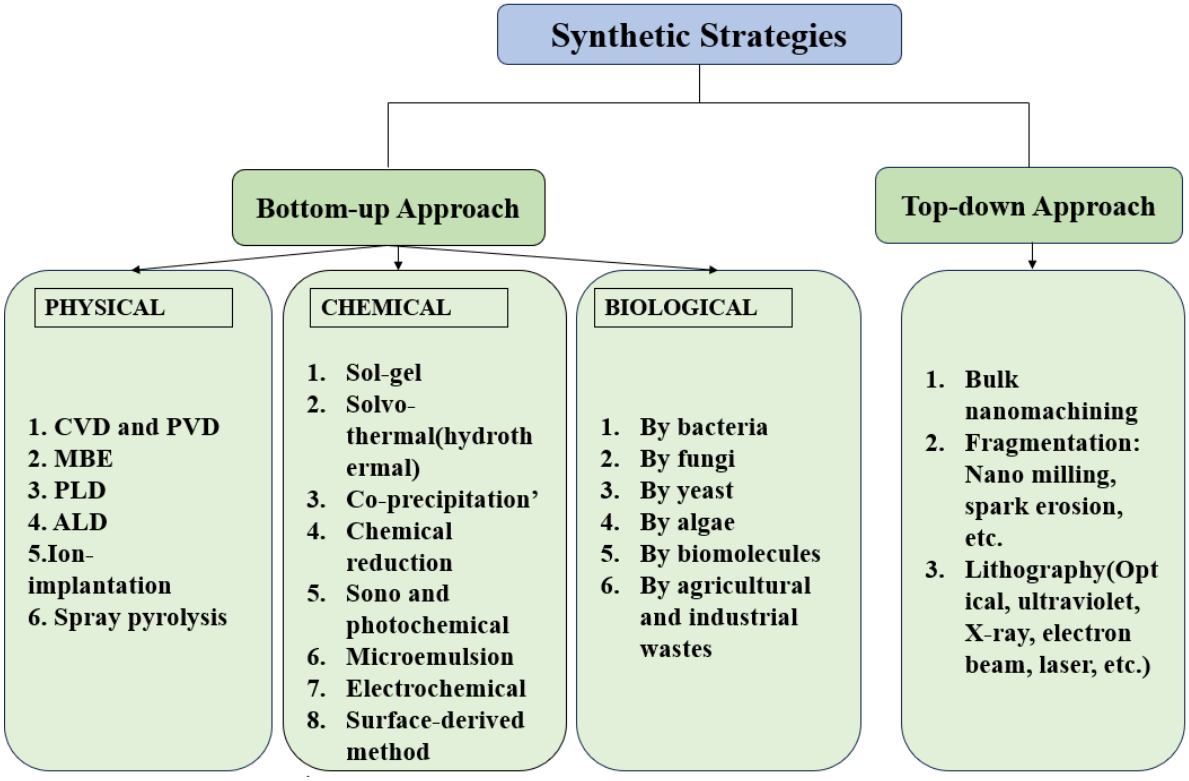

Fig. 1.2 Classification of Synthesis routes for nanomaterials.

Chemical synthesis is one of the most popular synthesis strategies for creating nanomaterials because of their ease of use, affordability, and capacity to regulate particle size and shape.

1.2.2 Applications of SnO_2

Gas Sensors

Gas sensors are the major application for SnO_2 nanomaterials. Tin oxide is highly responsive towards a wide variety of toxic and combustible gases such as H_2, CO, CH_4, NH_3, N_2O, ethanol and NOx. The basic principle for gas sensing is the change in electrical resistance due to the adsorption and desorption of gas molecules onto the surface of SnO_2 nanoparticles. The high surface-to-volume ratio of SnO_2 nanomaterials provides high interaction with gas molecules for good sensitivity and rapid response time. Therefore, SnO_2-based gas sensors are widely employed for air quality detection, industrial safety, domestic gas leak detection, environment

monitoring, etc. Compared to bulk materials, gas sensors utilizing nanostructured SnO in the form of nanowires, nanosheets, and nanoparticles display excellent sensing performance because nanoscale materials have more sites for adsorption [10].

Photocatalysis

SnO_2 nanomaterials have been utilized as effective photocatalysts for water purification and wastewater treatment. Upon irradiation, light creates electron-hole pairs within SnO_2, and subsequent redox reactions degrade organic pollutants and kill microorganisms. It is effective for the removal of colors, pesticides, and pharmaceutical contaminants from wastewater, as well as for removing poisonous organic substances from water. High stability against chemical attack makes it suitable for long-term application. It is often used in combination with other semiconductor materials as a heterojunction photocatalyst with better charge separation and visible light activity[11] .

Lithium-Ion Batteries

SnO_2 nanomaterials are used as the anode material for lithium-ion batteries owing to their high theoretical capacity and good performance. They react reversibly with Li+ during charging and discharging. High surface area provides a higher reaction surface area for faster Li+ diffusion and higher energy density. This would result in good capacity and cycling stability. Anode made from SnO_2 nanoparticles, nanofibers, and nanosheets has shown very high performance. Volume expansion during Li+ insertion still requires improvement using various compositing strategies [12].

Solar Cells

SnO_2 nanomaterials were used widely as transparent conductive electrode material and electron transport material in photovoltaic and solar cell devices due to their excellent transparency and conductivity. In dye-sensitised solar cells and perovskite solar cells, efficient electron transport is promoted by SnO_2 and charge recombination loss is reduced. The wide band gap of SnO_2 means high transparency in the visible light range, allowing most of the light to be absorbed by the active layer. Use of

nanostructured SnO_2 can also increase the efficiency and stability of the solar cell devices [13].

Transparent Conducting Electrodes

SnO_2 has good transparency and electrical conductivity; hence, it can be used as a transparent conductive electrode material. In liquid crystal displays, touch screens, display devices, smart windows, and transparent windows for buildings, SnO_2 films can be applied to a glass substrate. For optoelectronic devices, FTO(fluorine-doped tin oxide) can achieve higher conductivity with transparency. This has been widely used as a transparent electrode for solar cells, electrochromic devices, displays, sensors, etc [14].

Catalysis

SnO_2 nanomaterials have good catalytic and electrocatalytic activity due to their high surface area and active surface sites. They are used as catalysts and support for the reactions of oxidation, fuel cells, chemical synthesis, etc. In terms of catalytic application, SnO_2 nanomaterials can enhance the rate and selectivity of reactions. They offer high catalytic efficiency because of many sites for adsorption and reaction. They can also be used to decompose various harmful gases and pollutants [15].

Biosensors

SnO_2 nanomaterials were successfully used for biosensing applications owing to its good biocompatibility, high electron mobility and high reactivity. It helps the electron transfer between the electrode surface and biomolecules rapidly. The potential for application of SnO_2 nanomaterials is in glucose sensors, cholesterol sensors, DNA sensors, and other biomolecule sensors for health monitoring and diagnostics. It shows good sensitivity and fast response. By incorporating SnO_2 nanoparticles into biosensor platforms, high sensitivity and signal amplification were obtained [16].

Environmental Remediation

SnO_2 nanomaterials can be used as an effective tool for environmental purification. It possesses excellent photocatalytic and adsorption ability to decompose contaminants. By photocatalysis, the toxic organic compounds and pathogenic microorganisms were

removed from the wastewater; heavy metal ions were removed from the water, and toxic gases in the atmosphere were decomposed. Due to its stability and reusability. It is a good choice for sustainable environmental cleaning technology [17].

Optoelectronic Devices

SnO_2 nanomaterials are explored for application as optoelectronic devices such as UV detectors, light-emitting devices and photodetectors because of their good electron transport and wide band gap under UV light irradiation. They can be integrated into flexible electronics and transparent electronics because they have good mechanical strength and transparent properties [18].

Biomedical Applications

Some applications for biomedical fields have been explored, such as drug delivery carriers, antimicrobial coating and anticancer treatment. SnO_2 nanoparticles display antimicrobial properties against different pathogenic organisms. They can also make close contact with the biomolecules as the nanoscale materials, but more studies should be done on the toxicity and biocompatibility [19].

1.2.3 Co-precipitation Method

Among all wet chemical methods for synthesising SnO_2 nanoparticles and nanostructures, co-precipitation is considered the most popular one owing to its simplicity, low cost and easily controlled size and morphology of the particles. In this approach, a tin precursor salt like tin chloride ($SnCl_2$ or $SnCl_4$) is dissolved in distilled water to obtain a homogenous solution. The addition of a precipitating agent like sodium hydroxide (NaOH) or ammonium hydroxide (NHOH), slowly increases the solution pH, resulting in tin hydroxide precipitation.

The basic principle of the co-precipitation is the decrease in the solubility of metal ions in the solution. When the concentration of hydroxide ions is over the limit of solubility product, the tin ions react with the hydroxide ions, forming insoluble tin hydroxide precipitates as:

$$SnCl_4 + 4NH_4OH \longrightarrow Sn(OH)_4 + 4NH_4Cl \quad (1.1)$$

The precipitates are then filtered and washed multiple times so as to remove the impurities. Afterwards, the dried tin hydroxide precipitates were heated to high temperature, usually ranging from 400°C to 700°C, and converted to crystalline SnO_2 nanoparticles according to the reaction:

$$Sn(OH)_4 \xrightarrow{\Delta} SnO_2 + 2H_2O \quad (1.2)$$

The precipitation occurred via nucleation and particle growth mechanisms, where nuclei were formed first in the supersaturated solution, and they later grew into nanoparticles by diffusion and agglomeration. The size and morphology of SnO_2 nanoparticles synthesized by this method depend heavily on different parameters such as concentration of precursor salt, pH, reaction temperature, stirring speed, ageing time and calcination temperature [20]. Different nanostructures, including spherical nanoparticles, nanorods, nanoflowers, porous structures and nanoclusters, were achieved through tuning those parameters. High surface area and nanometer-scale grain size of the co-precipitated SnO_2 nanostructures are extremely beneficial for applications like gas sensing, photocatalytic and electrochemical applications. Low calcination temperature favours the formation of smaller particles and hence higher surface area, whereas increasing the calcination temperature might enhance crystallinity but tends to induce particle agglomeration. Co-precipitation is a simple, low-cost and well-suited method for large-scale preparation of SnO_2 nanostructures with good chemical homogeneity and high purity. There is no need for any special equipment, and dopants can easily be doped in the SnO_2 lattice to enhance the electrical, optical, and sensing characteristics of SnO_2. One of the limitations is the particle aggregation during the drying and calcination process; also, careful control of pH and washing conditions is crucial for the uniformity of nanoparticles. Due to all these advantages, co-precipitated SnO_2 nanostructures are being applied in gas sensors, Li-ion batteries, solar cells, transparent conductive films, supercapacitors, and photocatalytic degradation [21].

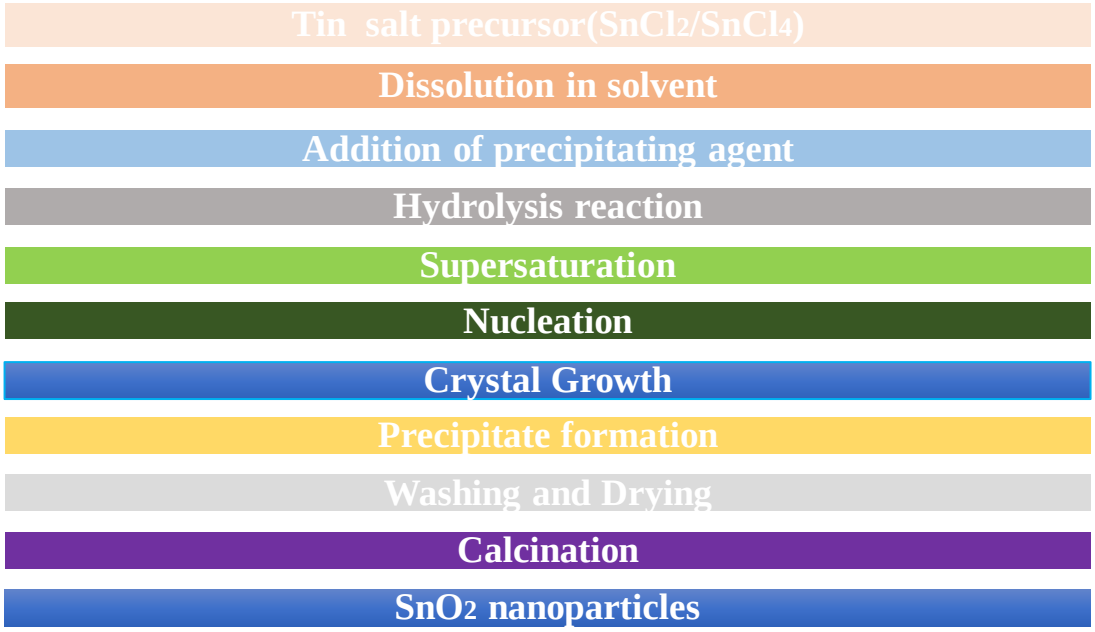

Fig. 1.3 General flowchart for the synthesis of SnO_2 by co-precipitation method.

1.2.4 Hydrothermal Method

The hydrothermal method is one of the most promising and popular strategies for preparing tin oxide nanostructures with controlled morphology, high crystallinity and good size uniformity. The hydrothermal method is a chemical method in which the reactions occur in a sealed vessel called an autoclave under high temperature and high pressure using an aqueous solution as a reaction medium. Due to the well-defined nanostructures that can be achieved under relatively low temperatures, the hydrothermal method is used in synthesizing SnO_2 nanoparticles, rods, wires, sheets, and complex micro and nano-structures.

The fundamental principle of the hydrothermal method is the increased solubility and reactivity of precursors in water at high temperature and high pressure. At high temperatures and high pressures, water is a potent solvent, and the solution is an active reaction medium, favouring nucleation and crystal growth. The tin precursors, such as $SnCl_5$. H_2O or $SnCl_2.H_2O$ were dissolved in distilled water. A precipitating or mineralising agent, such as NaOH, NH_4OH, or urea, was added to the solution to control the pH value. The obtained solutions were introduced into a Teflon-lined

stainless steel autoclave and heated at relatively low temperatures (commonly in the range of 120–220 C) for several hours [9].

The reactions occur at high temperature and pressure, which leads the tin ions in the solution to be hydrolyzed and react with hydroxide ions to form the tin hydroxide nucleus. Further crystal growth under hydrothermal conditions leads to highly crystalline SnO_2 nanostructures. The overall reaction processes were:

$$Sn^{4+} + 4OH^- \longrightarrow Sn(OH)_4 \qquad (1.3)$$

followed by thermal dehydration:

$$Sn(OH)_4 \xrightarrow{\text{Hydrothermal conditions}} SnO_2 + 2H_2O \qquad (1.4)$$

The growth of the SnO_2 nanostructures in the hydrothermal method is through the nucleation and growth mechanism. The precipitation process begins with nucleation, which forms the tiny nuclei. Then the nuclei grow slowly by dissolving and re-crystallization and through Ostwald Ripening, which allows them to grow into high crystalline nanostructures. The structure of the products is influenced by the synthesis parameters such as precursor concentrations, solution pH value, reaction temperature and duration, surfactants, and mineralizing agents. The most significant advantage of the hydrothermal method is the control over the shape and crystallinity of the product, it is suitable for obtaining a wide variety of SnO_2 nanostructures (nanoparticles, nanorods, nanoflowers, nanotubes, nanosheets, hollow spheres, complex structures, etc.). Higher reaction temperature and longer reaction time promote anisotropic crystal growth. Surfactants or capping agents help to direct the growth and control particle growth. Hydrothermally synthesized SnO_2 nanostructures possess high purity, uniform particle distribution, narrow size distribution, high surface area to volume ratio, which in turn boosts the sensing properties toward certain gases, photocatalytic performance, and optical and electrochemical characteristics of the materials, as these properties highly depend on the size and morphology of the nanoparticles. Larger surface area to volume ratio increases the gas adsorption and provides more active sites on the surface that can directly participate in gas sensing reaction or catalytic reaction. In comparison to the conventional synthesis method for nanostructures, such as high-temperature calcination in tube furnaces, the hydrothermal method has advantages like making

fully crystalline materials without annealing at extremely high temperatures. Besides that, it is a relatively simple and easy-to-handle, cost-effective, and environmentally friendly method that is available for synthesizing unique morphologies and shapes of nanostructures. Furthermore, it also allows the doping of metal elements and the formation of compounds easily by using various precursors. On the other hand, the main drawbacks were that it was difficult to scale up because of its limitations for the size of the autoclave used, and the reaction time was relatively long for complete reaction. Hydrothermally synthesized SnO_2 nanostructures have many applications such as gas sensors, rechargeable batteries, supercapacitor materials, solar cells, photocatalyst, transparent conducting films, and materials for environmental protection applications [22].

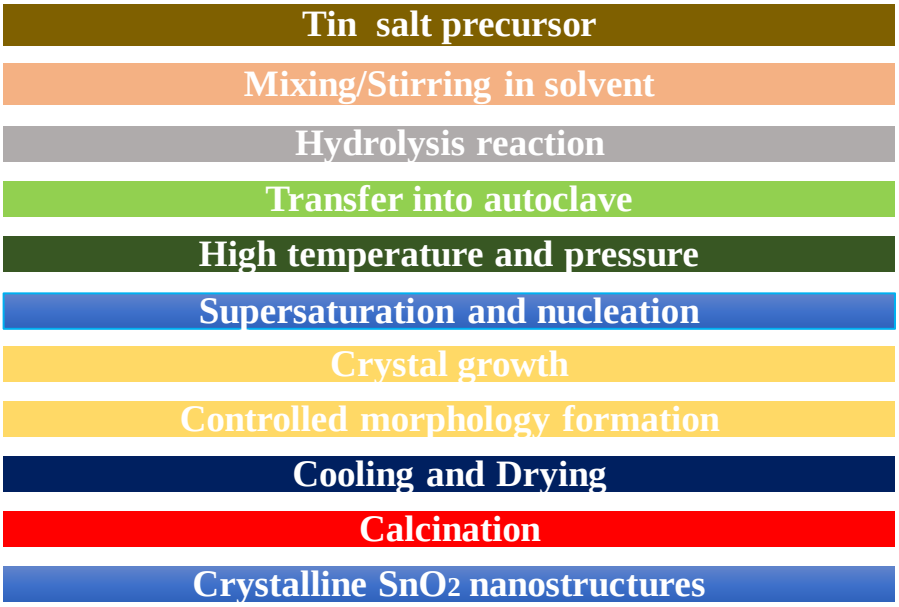

Fig. 1.4 General flowchart for the synthesis of SnO_2 by hydrothermal method.

1.3 SnS_2 nanomaterial

Tin disulfide (SnS_2) is a kind of important layered metal chalcogenide semiconductor and has attracted a great amount of attention due to its superior optical, electrical, photocatalytic, and electrochemical properties. The chemical formula of tin disulfide is SnS_2, where tin has +4 oxidation states and sulfur has 2 oxidation states. Typically, SnS_2 shows yellow or golden-yellow crystalline material, and it has good chemical and thermal stability. SnS_2 is an n-type semiconductor with a band gap in the range of

2.0-2.4 eV(shown in Fig. 1.5), depending on synthesis conditions, particle size, crystallinity and morphology. Since its band gap falls in the visible light region, SnS_2 can absorb visible light very well, and this is why it has potential for use in photocatalytic and photovoltaic applications. The relatively small band gap in comparison with many oxide semiconductors would help to achieve stronger visible light-driven charge carrier generation.

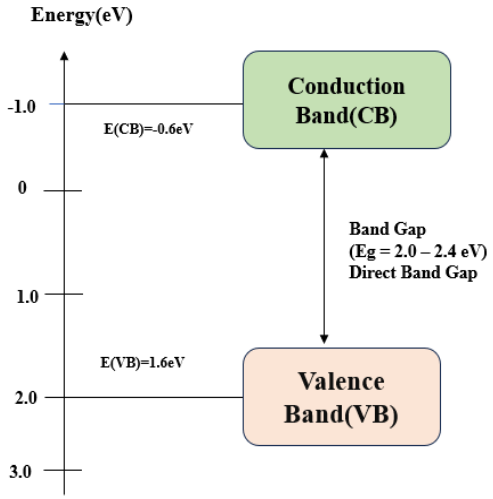

Fig. 1.5 Band Gap diagram of SnS_2

The structure of SnS_2 crystallizes with a hexagonal layered CdI-type crystal structure belonging to the P-3m1 space group. In this crystal structure, a layer of tin atoms is located between two layers of sulfur atoms, S-Sn-S layers, which are stacked together by weak van der Waals forces. The layered structure enables facile exfoliation into two-dimensional nanosheets and ultrathin layers of 2D nanostructures [23]. In order to achieve its highly anisotropic electrical and optical properties along different directions, it can exploit its own layer-structured property. The synthetic method to prepare the SnS_2 nanostructures includes hydrothermal, solvothermal, chemical vapour deposition, co-precipitation, microwave-assisted and sol-gel synthesis. The hydrothermal and solvothermal synthesis are the most used methods among those described above because they can control the morphology, high crystallinity and uniform distribution of particles. Different forms of SnS_2, such as nanosheets,

nanoflakes, nanoflowers, nanoplates, nanoparticles and hierarchical microspheres have been successfully synthesized by controlling the precursors' concentration, pH, temperature, reaction time, surfactants, and so on. The remarkable properties are shown by SnS_2: strong visible light absorption, good photoconductivity, large surface area (in nanostructured form), efficient charge transportation and excellent photocatalytic performance, etc. The layered structure facilitates the rapid separation and transfer of photogenerated electron-hole pairs, hence enhancing the photocatalytic and photoelectrochemical performance. The large surface area available in SnS nanostructures may act as a good platform to hold more active sites and promote the adsorption and catalytic activities. Based on those excellent properties, SnS_2 is widely investigated in applications including degradation of pollutants through photocatalysis, hydrogen generation, Li-ion battery, Na-ion battery, supercapacitor, photodetector, gas sensor and solar cell. SnS_2 can show remarkable efficiency in the degradation of dyes and environmental pollutants under visible light. In battery applications, the unique layer structure permits easy intercalation and high theoretical capacities[24].

1.3.1 Synthesis methods of SnS_2

For the synthesis of SnS_2 nanostructures, several approaches such as hydrothermal, solvothermal, co-precipitation, chemical vapour deposition (CVD), microwave-assisted and thermal decomposition methods have been reported. Morphology, particle size, crystallinity and surface area of SnS are highly sensitive to several parameters such as temperature, precursor concentration, pH, reaction time and surfactants used in synthesis processes. The hydrothermal method is one of the most widely used methods because it allows high control over morphology, crystallinity and size of nanostructures. In hydrothermal conditions, SnS_2 can be synthesized as nanobelts, nanosheets, nanoplates, nanoflowers and hierarchically organized microspheres. Smaller nanoparticles and ultrathin nanosheets are prepared at lower temperatures, whereas higher temperatures and longer reaction times promote a flower-like, layered structure with high crystallinity. This method is attractive because of its simplicity, low cost, eco-friendliness and capability of producing highly crystalline nanostructures with larger surface area and homogeneous morphology. Similar to the hydrothermal

method, in the solvothermal method, organic solvents are used instead of water [24]. It is useful for the synthesis of ultrathin layered nanosheets and well-defined flower-like structures with tunable thickness and enhanced optical properties. The co-precipitation is a simple and inexpensive wet chemical technique, where Sn-salts and S-precursors react with each other to form the precipitates of SnS_2. Nanoparticles and agglomerated grains with sizes between tens and ~100 nm are generally prepared via the co-precipitation method. The morphology control is rather limited compared to the hydrothermal method, but the co-precipitation method is very useful for industrial purposes because of its simple process, low cost, low reaction temperature, and scalability. CVD is generally applied for the fabrication of quality thin films and a 2D layer of SnS_2 nanosheets for optoelectronic and electronic devices. The microwave-assisted synthesis offers a method for the quick synthesis of uniform particles with a small size due to fast and homogenous heating. Among all these methods, hydrothermal and co-precipitation methods are the most attractive ones because they are simple, economical, require relatively less sophisticated equipment and also allow good control over particle size and morphology and thus produce well-crystalline nanostructures with large surface area, which are suitable for photocatalysis, electrochemistry, and energy storage applications [25].

1.3.2 Applications of SnS_2

The major applications of SnS_2 can be categorized as follows:

Energy Storage Devices:

SnS_2 has been applied in many electrodes such as those for lithium-ion battery, sodium-ion battery and supercapacitor due to its highest theoretical specific capacity and layered crystal structure. This layered structure permits fast insertion and extraction of ions during charging-discharging process, so as to improve the electrochemical performance. Moreover, the high surface area and the short diffusion pathways of ions of SnS_2 have contributed to energy storage efficiency, high charge capacity and excellent cyclic stability of devices. To enhance the conductivity and mechanical stability of SnS_2 for advanced battery devices, it is usually doped with carbon based materials, e.g. Graphene [26].

Photocatalysis:

SnS_2 has a suitable band gap and absorbs well in the visible light range and therefore serves as an efficient photocatalyst. Light-induced charge transfer of electron and hole pairs on the surface of SnS is beneficial for redox reactions. For this reason, SnS_2 has been employed in the degradation of hazardous organic dyes and pollutants contained in wastewater and research in photocatalytic water splitting to generate hydrogen as a clean and renewable energy source has been made by the team. High surface activity and good charge separation efficiency also promote the photocatalytic ability of SnS_2 [27].

Gas Sensors:

SnS_2 nanostructures are known to be highly sensitive towards a variety of toxic and flammable gases such as NO, NH_3, ethanol vapour, and H_2S. When those gas molecules adsorb to the surface of SnS, the resistance of the material will vary due to a change in electron concentration. Because of the large surface to volume ratio, high sensitivity and fast response to toxic gases at low concentrations, SnS_2 is regarded as a promising sensing material for air-quality monitors and other applications for environmental sensing, industrial safety, etc [28].

Solar Cells and Optoelectronic Devices:

SnS_2 exhibits excellent optical and semiconducting characteristics with a suitable band gap, high absorption coefficient and good carrier mobility, so it has been widely used in thin-film solar cells in which light harvesting and energy conversion can be highly efficient. Apart from this, SnS_2 is also useful for photodetectors, phototransistors, field-effect transistors and so on. Furthermore, due to its 2D layer structure and nanoelectronic feature, SnS_2 may also find some applications [29].

Lubricants and Tribological Applications:

The layered crystalline structure allows sliding between layers to minimize friction, therefore, SnS_2 is useful as solid lubricant in mechanical and industrial systems at high temperature or vacuum condition since liquid lubricant usually fail at such condition, thus preventing wear and increasing service life of components [30].

Biomedical Applications:

Recent work revealed the potential of SnS_2 nanostructures in the biomedical field based on their unique optical and surface characteristics. The use of SnS_2 nanomaterials for the development of drug delivery systems, bioimaging and anti-bacterial materials and photothermal therapy has been studied. The high surface area of the SnS_2 nanostructures is good for carrying drug molecules, and its optical property is useful for imaging. The research is, however, still mainly in the laboratory stage [31].

1.3.3 Co-precipitation Method

A facile, inexpensive and widely used wet chemical synthesis method for preparing SnS_2 nanoparticles and nanostructures is the co-precipitation method. This method involves the formation of an insoluble SnS_2 precipitate from a homogeneous solution of Sn and S ions. A Sn precursor, such as SnCl, is dissolved in water, and then a sulfur source, such as thiourea or sodium sulfide, is added slowly to the solution with constant stirring. Once the sulfur ion concentration is beyond the solubility of the SnS_2 particles, Sn ions and S ions get precipitated as SnS_2. The following reaction can be represented.

$$Sn^{+4} + 2S^{2-} \longrightarrow SnS_2 \qquad (1.5)$$

The precipitation happens in the processes of nucleation and growth of the particles. At the beginning, a small nucleus of SnS_2 particles is formed by the supersaturation of ions. Particles start growing further through the aggregation of particles. Control over parameters like pH, precursor concentration, temperature, speed of stirring, calcination temperature, etc., plays an important role in the determination of particle size and morphology. This method has resulted in nano-sized particles and aggregated nano-clusters and grains with a size in the range of a few nanometers to close to 100nm. For a lower precursor concentration and under control of pH values, the particle size may be significantly reduced, whereas an increase in calcination temperature provides higher crystallinity, which tends to increase the aggregation of particles. An advantage of using the co-precipitation method for SnS_2 nanomaterials preparation is: low cost, low temperature of the reaction and suitability for large-scale production. The experimental setup required is simple and not very expensive. This method provides a

homogeneous mixture of the starting elements and also a large surface area of the resultant nanomaterials. For these reasons, co-precipitated SnS_2 nanomaterials are used in various applications such as photocatalysis, gas sensors, lithium-ion batteries, supercapacitors, and solar cells, etc [32].

1.3.4 Hydrothermal Method

The hydrothermal method is one of the most commonly used techniques for synthesizing SnS_2 nanostructures owing to its good controllability in particle size, morphology, crystallinity and surface area. In this method, tin and sulfur precursors are dissolved in water, and the mixture is then kept in a sealed Teflon-lined autoclave and heated at a higher temperature and pressure. Typical tin precursor is tin chloride, while sulfur precursor is generally thiourea or thioacetamide. The principle of the hydrothermal method relies on crystal growth under a high-temperature and high-pressure aqueous system. Hydrothermal conditions improve the solubility and reactivity of precursors, which in turn enhance the nucleation and controlled crystal growth of SnS_2 nanostructures.

The schematic reaction can be written as:

$$Sn^{4+} + 2S^{2-} \longrightarrow SnS_2 \qquad (1.6)$$

Formation of SnS_2 involves nucleation and growth processes. Nanoparticles of different sizes form when the solution reaches supersaturation. These nanoparticles grow further to different nanostructures depending on reaction conditions such as temperature, precursor concentration, reaction time, pH and surfactants. The hydrothermal method can produce different morphologies such as nanosheets, nanoplates, nanoflakes, nanoflowers, nanobelts, and hierarchical microspheres. Smaller-sized nanoparticles and ultrathin nanosheets can be formed at low temperature and short reaction time, while flower-like and layered structures can be obtained with better crystallinity at higher temperature and long reaction duration. Surfactants such as CTAB and PVP are used to control the morphology and suppress agglomeration. One of the main advantages of the hydrothermal method is that it produces nanostructures with highly crystalline and uniform with a high surface area at relatively low temperatures. This method is simple, environmentally friendly,

economical, and controllable, yielding different morphologies [33]. Hence, the hydrothermally synthesized SnS_2 nanostructures find extensive application in photocatalysis, lithium-ion battery, supercapacitor, gas sensor, hydrogen generation and solar cell.

CHAPTER-2

MATERIALS AND METHODS

2.1 MATERIALS USED

1. FOR SnO_2 SYNTHESIS BY CO-PRECIPITATION METHOD: Tin Chloride Pent Hydrate($SnCl_4.5H_2O$), Ethanol, Ammonia.

2. FOR SnO_2 SYNTHESIS BY HYDROTHERMAL METHOD: Tin Chloride Pent Hydrate($SnCl_4.5H_2O$), NaOH, Ethanol.

3. FOR SnS_2 SYNTHESIS BY CO-PRECIPITATION METHOD: Tin Chloride Pent Hydrate($SnCl_4.5H_2O$), HCl, Thioacetamide.

4. FOR SnS_2 SYNTHESIS BY HYDROTHERMAL METHOD: Tin Chloride Pent Hydrate($SnCl_4.5H_2O$), Thiourea

2.2 SYNTHESIS METHODS

2.2.1 CO-PRECIPITATION SYNTHESIS OF SnO_2

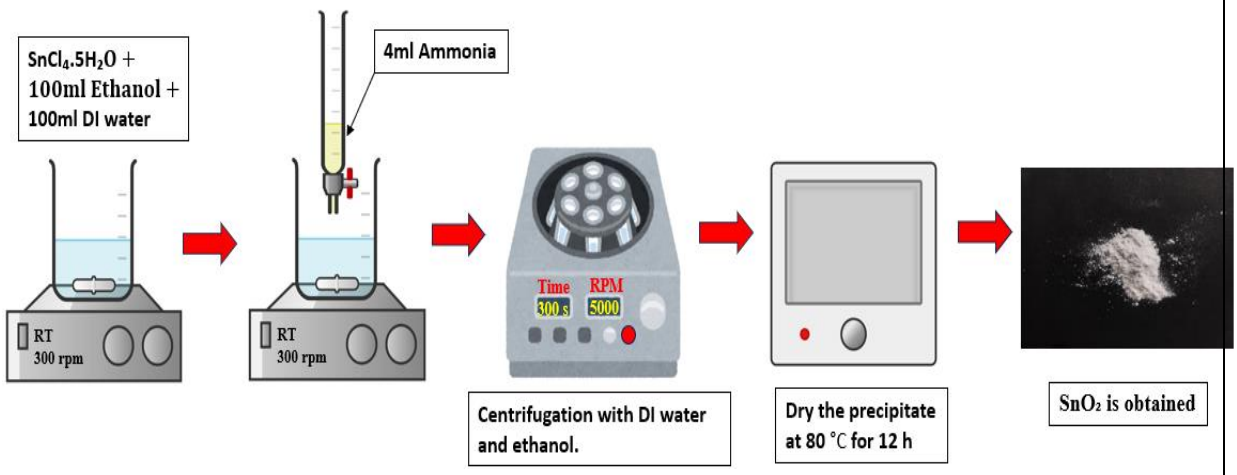

Fig. 2.1 Schematic illustration of SnO_2 synthesis via the Co-precipitation method

SnO_2 nanomaterials were prepared by the chemical co-precipitation method. Firstly, 3.5 g of $SnCl_4.5H_2O$ was dissolved in 100 mL of DI water, and then 100 mL of ethanol was added. Then the solution was stirred on a magnetic stirrer for 30 minutes at 300rpm. Further, 4 mL of an aqueous ammonia solution was added @10 drops/minute to the above solution with continuous stirring. Throughout this procedure, the dropping rate was carefully managed to ensure chemical uniformity and produce a white slurry. The resulting mixture was spun in a centrifuge and gathered, then rinsed with deionized water to eliminate impurities. Then dry the precipitate at 80 ºC for 12 h and calcinate at 230 ºC for 2 h. At last, the sample was ground to obtain a fine SnO_2 powder [34]. Fig. 2.1 shows the synthesis process of this method.

2.2.2 Synthesis of SnO_2 by Hydrothermal Method

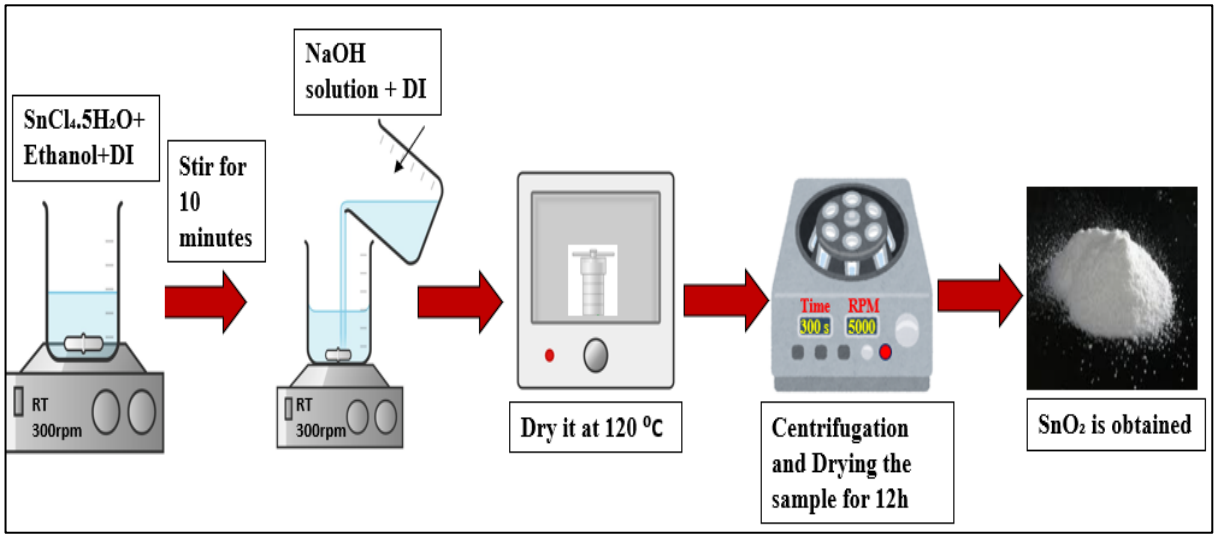

Fig. 2.2 Schematic illustration of SnO_2 synthesis via the hydrothermal method

SnO_2 nanoparticles were synthesized by using the hydrothermal method. In this process, 5.609 g of $SnCl_4.5H_2O$ (0.12 M) was mixed with a 1:1 weight ratio of ethanol and DI water (25ml ethanol and 25 mL DI). Then, the solution was stirred for 10 minutes. Simultaneously, 0.67 g of NaOH solution is mixed in 25 mL of DI using the sonication method. Now, this NaOH solution is added slowly into the above solution, and 25 mL of DI water is added during stirring. The mixture was stirred for 10 minutes and then transferred to a 100 mL autoclave. The autoclave was placed in an oven under reaction temperature at 120 °C for 18 h. The resulting precipitate was centrifuged and washed with DI water and ethanol, and then dried for 12 h [35]. Now, the sample was ground to obtain the final product. Fig. 2.2 shows the synthesis process of this method.

2.2.3 Synthesis of SnS_2 by Co-precipitation Method

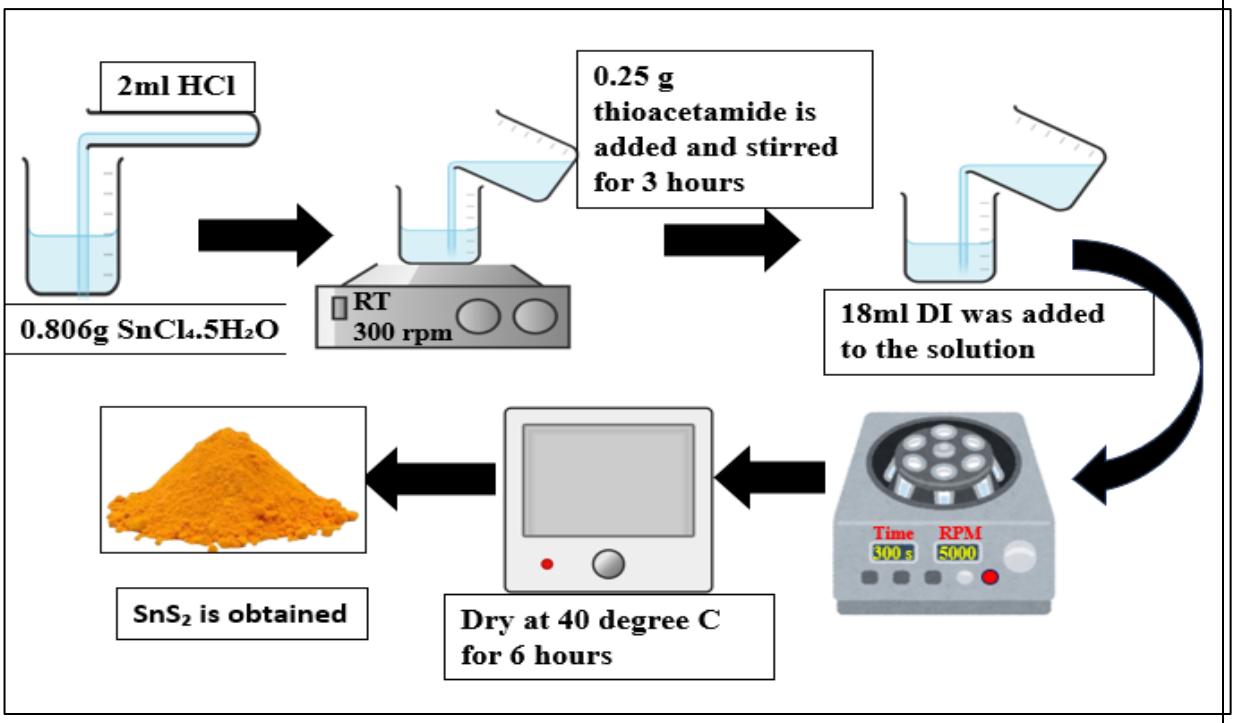

Fig. 2.3 Schematic illustration of SnS_2 synthesis via the Co-precipitation method

SnS_2 nanoparticles were synthesized by the co-precipitation method. SnS_2 synthesis involved dissolving 0.806 g of $SnCl_4 \cdot 5H_2O$ in 2 mL of concentrated HCl. Following 5 minutes of stirring, 30 ml of deionized water was added to the solution. Next, 0.25 g of thioacetamide was added, and the mixture was stirred for 3 hours. Afterwards, the solution was brought to a final volume of 50 mL with the addition of 18 mL of deionized water. After letting the mixture rest for 30 min, a yellow precipitate was formed, and it was centrifuged with DI and ethanol [36]. Then dry this obtained product at 40 ºC for 6 h. Crush the sample into fine powder. A yellow powder is obtained. Fig. 2.3 shows the synthesis process of this method.

2.2.4 Synthesis of SnS_2 by Hydrothermal Method

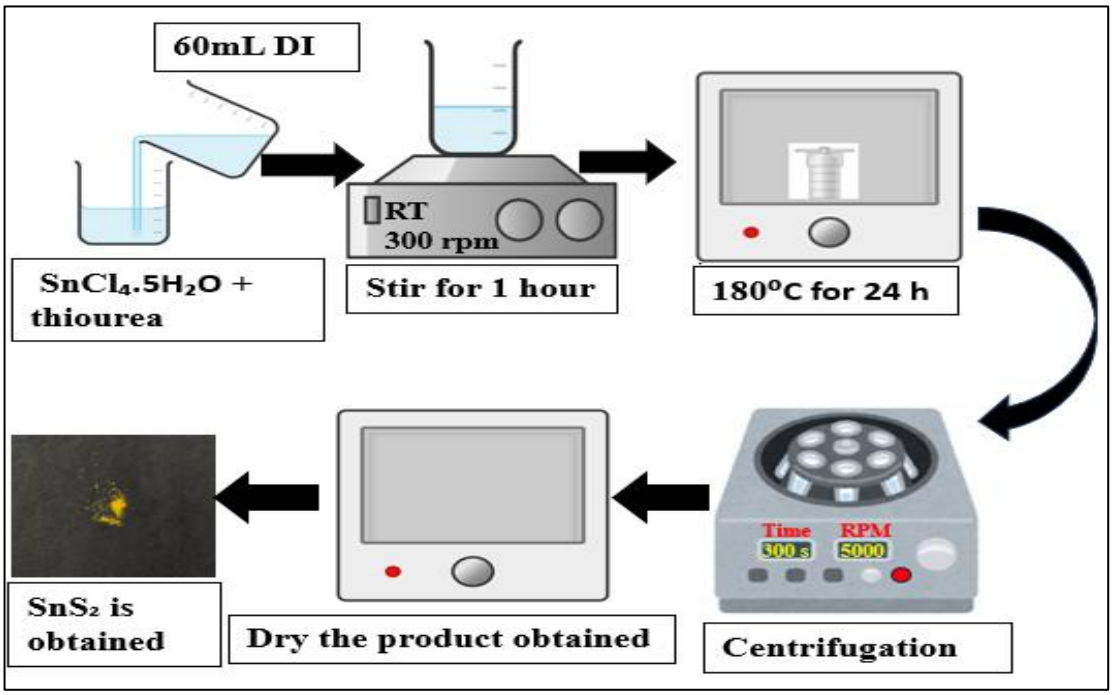

Fig. 2.4 Schematic illustration of SnS_2 synthesis via the hydrothermal method

500 mg of $SnCl_4 \cdot 5H_2O$ and 1000 mg of thiourea were dissolved in 60 mL of DI water. Stir the mixture for 1 h. Subsequently, the prepared solution was moved to a 100 mL Teflon vessel and maintained at 180 °C for 24 hours. Afterwards, the solution was allowed to cool to room temperature. Next, the sample was centrifuged with deionized water and ethanol. Then dry the obtained product at 60 °C for 24 h, which yields a yellow powder [37]. Fig. 2.4 shows the synthesis process of this method.

CHAPTER -3

CHARACTERIZATION AND RESULTS

3.1 CHARACTERIZATION TECHNIQUES

3.1.1 X-RAY DIFFRACTION

X-ray diffraction (XRD) is one of the essential analysis techniques employed for characterization of the structure of crystalline materials. Through XRD analysis, it is possible to determine the crystal structure, the phase composition and lattice parameters, the crystallite size and the orientation of materials. This method is widely applied in the fields of physics, chemistry, nano-technology, metallurgy and material science, owing to its precise and non-destructive features. The working principle of XRD is based on the interaction between X-rays and the regularly placed atoms of the crystal [38].

Principle of X-Ray Diffraction

When a monochromatic beam of X-rays strikes a crystalline material, the X-rays get scattered in different directions by atoms in the crystal. As the atoms are regularly placed in planes in a crystal, these scattered waves interfere with each other. For certain specific angles, there is constructive interference of the waves, which leads to a peak reflected ray called a diffraction peak. This condition is described by Bragg's law.

Bragg's Law: The condition required for diffraction is, in mathematical terms.

$$n\lambda = 2d\sin(\theta) \tag{3.1}$$

Where:

n=Order of diffraction

λ=wavelength of incident X-rays

D=spacing between crystal planes

θ=angle of incidence

From Bragg's law, diffraction will take place if, and only if, the difference in path lengths between X-rays reflected from successive crystal planes equals an integral multiple of the wavelength. In this situation, constructive interference occurs, and an intense diffracted beam is generated. The extra distance travelled by the reflected X-rays from the adjoining planes is equal to 2dsinθ [39]. Thus, the condition required for diffraction is equal to.

$$2d\sin(\theta) = n\lambda \qquad (3.2)$$

This is the basis of X-ray diffraction.

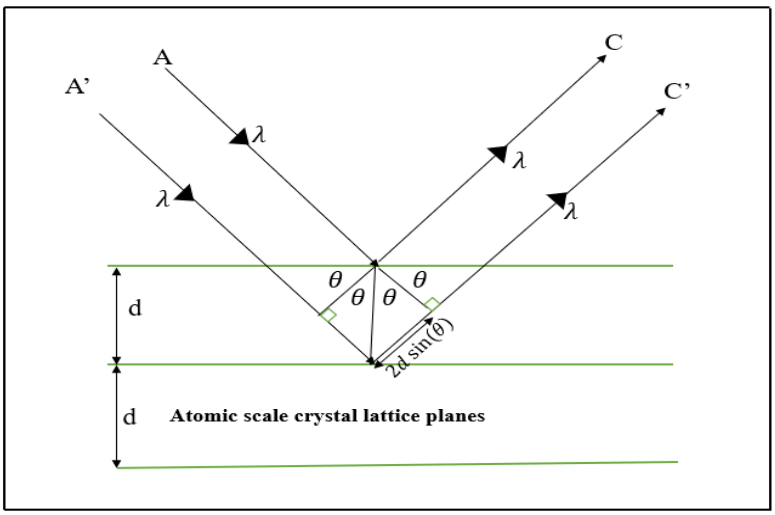

Fig. 3.1 Bragg's Law

Working:

The X-rays are produced by a source such as a metal target, usually copper, within an X-ray tube. This then gets monochromatic by a filter or analyser, and gets collimated to form a narrow X-ray beam that will hit the crystal specimen situated at the specimen holder. The beam can be diffracted from the crystal, because of the crystal's regular atomic structure, at several angles following Bragg's condition. The detector can scan around the crystal, and the diffracted intensity is collected at different angles of diffraction, 2θ. An XRD pattern or diffractogram is plotted of intensity as a function of the diffraction angle, 2θ, and this reveals information about the crystal structure or the phase composition .

Scherrer equation:

Crystallite size for nanomaterials can be calculated from X-ray diffraction data using the following Scherrer equation: In an X-ray diffraction pattern, diffraction peaks broaden with decreasing crystallite size. Smaller crystallites have wider diffraction peaks, whereas the larger crystallites have sharper diffraction peaks.

It can be represented as:

$$D = \frac{k\lambda}{\beta \cos\theta} \qquad (3.3)$$

Here:

D = average crystallite size.

K = shape factor for the particle, which is 0.9 in general.

λ= wavelength of X-rays (which is commonly 0.1541nm for Cu Kα radiation.

β= full width at half maximum (FWHM) in radians.

θ = Bragg diffraction angle.

The Scherrer equation is used widely in nanotechnology and material science. It provides a rough estimation for calculating crystallite size of nano-particles, thin films, etc., from the XRD pattern [40].

3.1.2 Field Emission Scanning Electron Microscopy

Field Emission Scanning Electron Microscopy (FESEM) is an advanced type of electron microscopy that provides images with much higher resolution on the surface structure and microstructure of the materials. It is extensively used in nanotechnology, material science, physics, chemistry, metallography and biological science for the characterization of nanoparticles, thin films, nanocomposites, and crystalline materials. It can be used for the analysis of the size, shape, texture and surface features of material at the nanometer scale. The FESEM makes use of a field emission electron source, which provides a fine focused beam of electrons of very small diameter and of higher brightness in comparison to the traditional scanning electron microscopy(SEM). FESEM can produce better images with a larger depth of field and a clearer surface picture [41].

Principle of FESEM

The working of FESEM relies on the interaction between highly accelerated electrons focused into a beam and surface atoms of the specimen. The impact of the electron beam on the sample surface excites various signals like secondary electrons, backscattered electrons, and characteristic X-rays through interaction with matter.

These emitted secondary electrons are the primary signals that are used for imaging, because the surface morphology and topography of the material are displayed in images generated by these secondary electrons. The intensity of emitted electrons is proportional to the surface structure of the specimen. Thus, FESEM produces images with higher magnification and good resolution .

In FESEM, electrons are obtained by field emission from a pointed tungsten filament by applying a high electric field. After this, electrons are accelerated and focused by electromagnetic lenses to a fine beam. This beam is scanned in the raster pattern over the specimen surface, then all the signals obtained are displayed on the display by converting them to image signals.

Working:

FESEM utilizes field emission of electrons from an electron gun. These electrons are accelerated at a high voltage and passed through electromagnetic condenser lenses that focus the beam to a small point. The electron beam then scans the sample surface line by line. When electrons strike the sample, secondary electrons and backscattered electrons are produced. Detectors collect the emitted electrons, and the intensity of the signal is processed by a computer to produce a magnified image of the sample surface. High vacuum is maintained throughout the system so that the electrons are not scattered by gas molecules. If a non-conductive sample is used, then the sample is often coated with a thin conductive layer of gold or platinum [42].

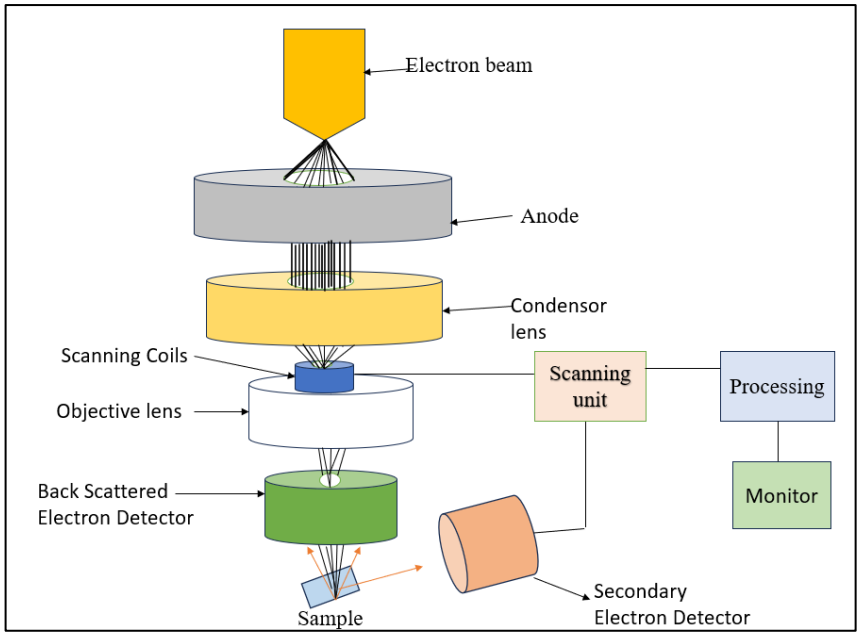

Fig. 3.2 FESEM schematic diagram

Morphology and microstructure information of materials can be identified by FESEM. The size of particles, grain size, shape of particles, roughness of surface, porosity, crack, defects, agglomeration of particles, etc., can be seen by FESEM. With the help of FESEM, the uniform distribution and morphology of nanoparticles in thin films and nanocomposites can be determined. Also, the compositional contrast between different areas of a sample can be observed by back-scattered electron imaging. If EDX (EDS) is employed with FESEM, it is possible to analyze the elemental composition and chemical state of a material.

Energy Dispersive X-Ray Spectroscopy

Energy Dispersive X-ray Spectroscopy is an important analytical technique for the elemental and composition analysis of samples. It is usually equipped with SEM or FESEM system for composition determination of the sample. The principle of the method is that when a high energetic electron beam strikes the surface of a sample, characteristic X-ray will be produced from atoms present in the material. Each element will produce X-rays with certain energies. Hence, these signals will indicate elements present in the sample. It gives qualitatively and quantitatively elemental composition, atomic and weight percentage, detection of dopant and presence of impurities within nanoparticles and thin films. EDX analysis gives element mapping, in which elemental composition across the sample surface is clearly demonstrated. Coupled with FESEM, it provides both morphology and composition information. So EDX is a very helpful tool to characterization of nanomaterials, thin films, nanoparticles, alloys, ceramics, composite materials, semiconductor devices and in other fields of nanotechnology and material science [43].

3.1.3 Fourier Transform Infrared Spectroscopy

FTIR is a common and valuable technique for chemical bond identification, functional group and molecular structures determination of materials. The technique is the interaction of infrared radiation with matter. It finds common use in fields such as physics, chemistry, nano-science and technology, material science, pharmaceutics, polymers and biological sciences for both qualitative and quantitative analysis of materials. Every molecule will vibrate with its own characteristic frequencies; when infrared radiation is passed through a sample, specific frequencies are absorbed by the molecules, which in turn cause stretching and bending of chemical bonds. This causes an infrared spectrum, which serves as a fingerprint for that molecule. FTIR can therefore be very useful in determining compounds and their respective interactions.

Principle of FTIR

The molecules in the sample will absorb the infrared radiation. When infrared radiation falls on the materials, the molecules will absorb energy corresponding to their vibrational frequencies. Characteristic vibration frequencies are particular to a certain

type of chemical bond. The absorption results in vibration transitions. Such transitions include vibration-rotation transitions in gas, vibrational modes in solid/liquid. They are represented as vibration types: stretching vibration, bending vibration. The detected values will be the infrared spectrum, which corresponds to the specific absorbed frequencies.

The relationship between frequency and wavelength is given as:

$$\upsilon = \frac{1}{\lambda} \qquad (3.4)$$

Where: υ is the wave number and λ is the wavelength.

FTIR spectrum represents the absorbance/transmittance against the wave number (usually plotted in a certain wave number range, like 400 to 4000cm^{-1}). There is an absorption peak corresponding to a functional group in the sample [44].

Working:

In FTIR spectroscopy, the infrared radiation from the source is incident on an interferometer. The beam splitter divides the radiation into two beams, one to a fixed mirror and the other to a moving mirror. The two beams are then recombined to form an interference pattern called an interferogram. The interferogram is incident on the sample, where some of the frequencies are absorbed by the sample. The beam that passes through the sample is incident upon the detector and produces an electrical signal. The computer then takes a Fourier transformation of the interferogram to produce the final infrared spectrum [45].

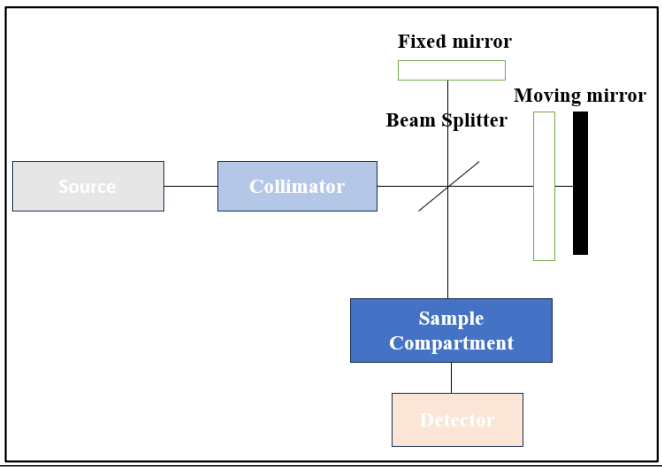

Fig. 3.3 Schematic Diagram of FTIR spectroscopy

3.1.4 UV-Visible Spectroscopy

Spectroscopic methods are valuable for material characterization as they provide an insight into structure, electronic and optical properties. UV-Visible (UV-Vis) spectroscopy is one of the most popular analysis techniques for the study of the interaction between electromagnetic radiation and materials. In UV-Vis spectroscopy, absorption or transmission of UV and visible region radiation through a sample is observed. The electron absorption of a definite amount of energy for a particular wavelength makes it jump to higher energy levels from the ground states. The resultant spectrum yields important information about electronic structure, optical transition, concentration and band gap energy of the material. For materials science and nanotechnology it is applied to characterize semiconductors, nanoparticles, thin films, polymers and metal complexes. It is easy, fast, non-destructive and very sensitive for both qualitative and quantitative studies. In this work, the optical properties of the prepared samples are determined using UV-Vis spectroscopy, and the optical band gap energy is calculated using this method [46].

Principle

UV-Visible spectroscopy is a way to figure out how ultraviolet and visible radiation a substance absorbs at different wavelengths. This technique is based on what happens when molecules or substances take in radiation. When this radiation hits a substance, it makes an electron move to an energy level from a lower one because of the energy it takes in. UV-Visible spectroscopy looks at the range, which is from 200 to 400 nanometers and the visible range, which is from 400 to 800 nanometers. UV-Visible spectroscopy is really useful for understanding how substances react to visible radiation. The electron transitions are of different types, such as:

$\pi \longrightarrow \pi^*$ transitions

$n \longrightarrow n^*$ transitions

d-d transitions (in transition metal complexes)

Charge transfer transitions

Working

UV-Vis spectroscopy involves passing a beam of light from the UV and Visible regions through a solution sample. This helps in finding the extent of light absorbed by the sample. Initially, the light from the source is passed to the monochromator that selects the individual wavelength by separating the whole light of all individual wavelengths. The light sources used are a Deuterium lamp for the UV region and a Tungsten lamp for the visible region. The individual monochromatic light rays are then allowed to pass through a solution sample placed in a cuvette. The molecule present in the sample absorbs some amount of light. Due to absorption of energy, there occur electronic transitions within molecules; the electrons absorb energy and jump from lower energy levels to higher energy levels. The unabsorbed light rays pass through the solution sample and reach the detector. The detector converts the light to an electrical signal, which is then interpreted by the instrument, and a comparison of the intensity of light passing through the sample to that entering the sample is made to determine the absorbance of the solution. The absorbance value is then obtained in the form of a spectrum, a graph of absorbance versus wavelength.

The concentration of the substance can be determined by Beer-Lambert's law:

$$A = \in cl \qquad (3.5)$$

Where A is absorbance, ∈ is molar absorptivity, c is concentration, and l is path length.

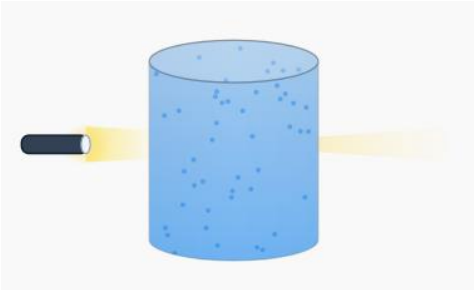

Fig. 3.4 Schematic representation of absorption of light by the sample

UV-Vis spectroscopy has broad applications, including the determination of the concentration of substances, the identification of nanoparticles, and also to find the

electronic properties of materials. The absorption pattern gives an idea of the electronic structure, optical properties, concentration, and band gap of the substance [47].

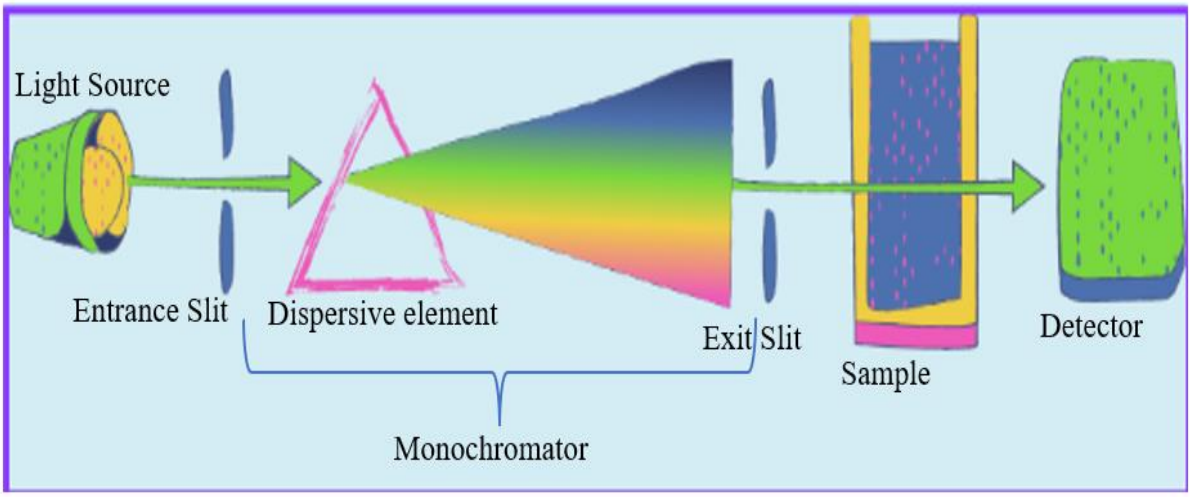

Fig. 3.5 Schematic diagram of UV- Visible spectroscopy

3.2 Results and Discussion

3.2.1 XRD

3.2.1.1SnO_2 by Co-precipitation Method and Hydrothermal Method

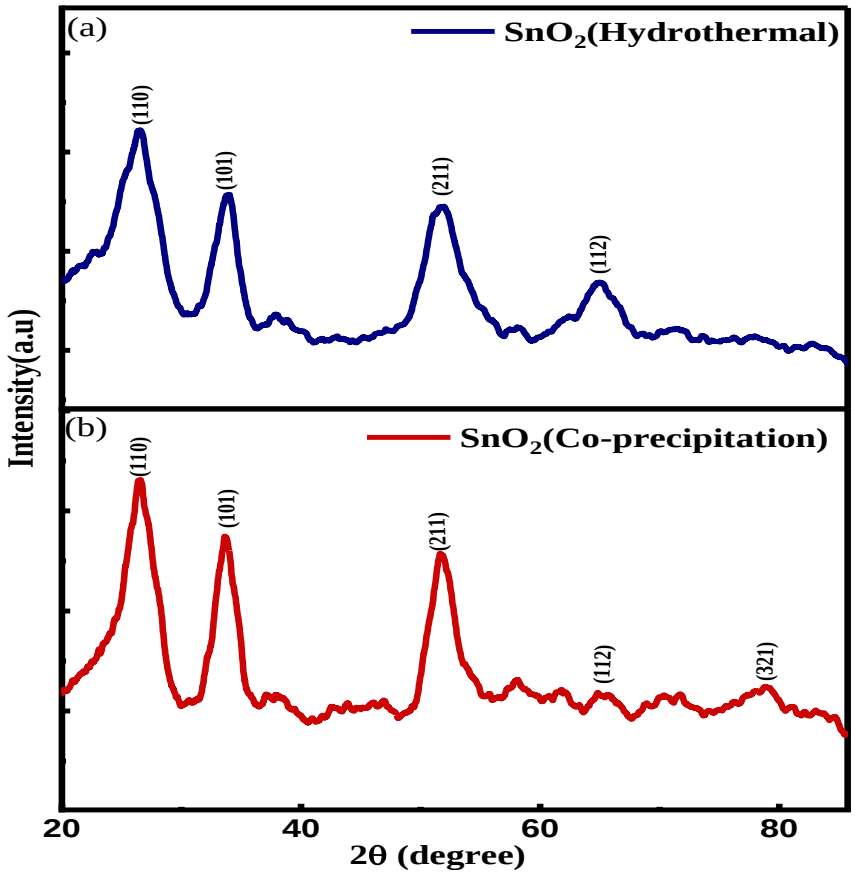

Fig. 3.6 XRD of SnO_2 made by (a)Co-precipitation method (b) Hydrothermal method

Fig. 3.6 shows the XRD pattern of the SnO_2 synthesized via the co-precipitation and hydrothermal method. It shows that all the peaks of SnO_2 are in good agreement with the standard JCPDS card no 00-041-1445. X-Ray Diffraction study confirmed the formation of SnO_2 nanostructures with a tetragonal rutile crystal structure [48]. On comparison of both methods, for SnO_2 synthesized by co-precipitation, the diffraction peaks were observed at 26.4º (110), 33.6º (101), 51.66º (211), 64.84º (112), and 79.06º (321). These peaks showed high sharpness, which indicates better crystallinity. For the

hydrothermal sample, the diffraction peaks were seen at 26.54º (110), 33.78º (101), 51.6º (211), and 64.92º (112). These peaks were comparatively broader, which indicates a smaller crystallite size and reduced crystallinity. The crystallite size(D) was calculated using the Scherrer equation (Eqn 3.6).

$$D = \frac{k\lambda}{\beta \cos\theta} \qquad (3.6)$$

Here, D is the average crystallite size, K is the shape factor, which is equal to 0.9, λ is the X-Ray wavelength, θ is the Bragg diffraction angle of the diffraction peaks, and β gives the full width of the half maxima (FWHM). Analysis using the Scherrer equation revealed an average particle size of 3.019 nm for the co-precipitation sample and 1.43 nm for the hydrothermal sample, notably smaller in comparison. The value of d-spacing of the most intense peaks for both methods is 0.34 nm, which matches the JCPDS card no. 00-041-1445. It concludes that the co-precipitation method produces higher crystallinity and larger crystallite size because, in this synthesis, we synthesize nanomaterials at room temperature, while in the hydrothermal method, we synthesize the material at high temperature and pressure, resulting in a smaller crystallite size [49]. There is an increase in nucleation at higher temperature and pressure, which also results in a smaller crystallite size. In contrast, co-precipitation involves controlled nucleation and significant post-precipitation growth and agglomeration, which result in a larger crystallite size [50].

3.2.1.2 SnS_2 by Co-precipitation and Hydrothermal method

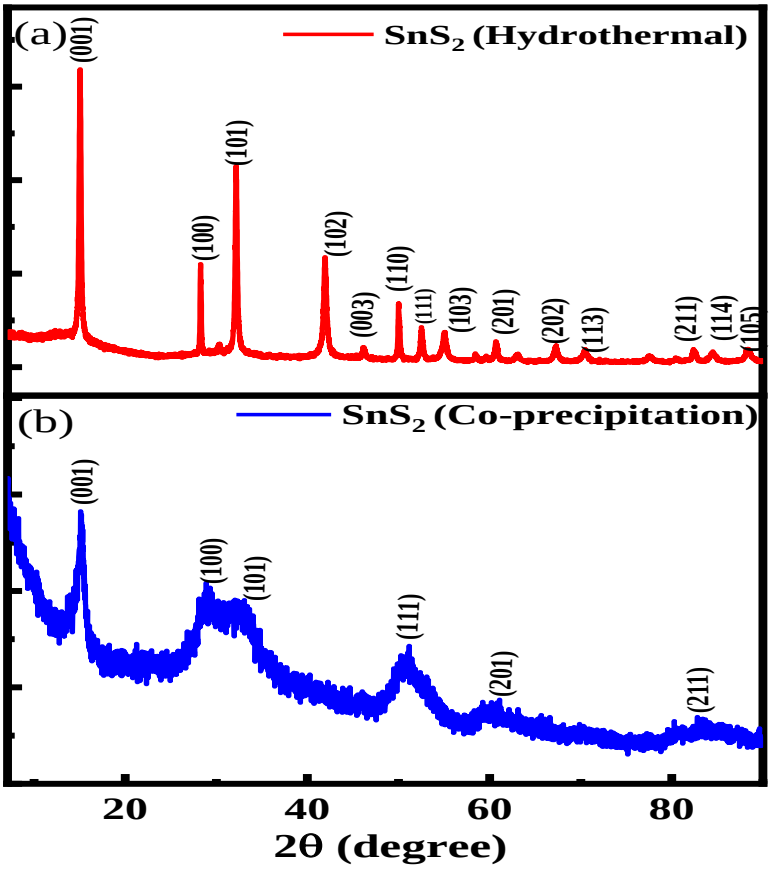

Fig. 3.7 XRD of SnS_2 made by (a)Co-precipitation method (b) Hydrothermal method

For SnS_2, the peaks were well matched with the JCPDS card no. 00-023-0677. SnS_2 has a layered hexagonal structure [51]. For the co-precipitation method, the diffraction peaks were observed with 2θ values at 15.18º (001), 28.9º (100), 33.88º (101), 51.18º (111), 54.98º (201), and 82.82º (211). These peaks showed the formation of crystalline SnS_2 with moderate intensity and crystallinity. For the hydrothermal method, the diffraction peaks were observed at 15.04º (001), 29.57º (100), 32.17º (101), 41.93º (102), 46.08º (003), 50.01º (110), 52.51º (111), 55.03º (103), 60.68º (201), 67.30º (202), 70.49º (113), 82.37º (211), 84.49º (114), and 88.22º (105). Here, more peaks are showing better phase formation and higher crystallinity. The smaller the crystallite size, the lower the crystallinity of the material [52]. Crystallite sizes were measured at 8.07 nm for the co-precipitation sample and 32.98 nm for the hydrothermal sample.

The value of d-spacing of the most intense peaks for both methods is 0.59 nm, which matches the JCPDS card no. 00-023-0677. Hydrothermal synthesis of SnS_2 involves nucleation, which causes growth, aggregation, and Ostwald ripening, resulting in the enlargement of crystallite size over time. In contrast, precipitation-based methods involve rapid nucleation under high supersaturation, resulting in a large number of nuclei and limited growth per particle, which results in smaller crystallite sizes due to kinetic control and restricted diffusion [53].

3.2.2 Field Emission Scanning Electron Microscopy (FESEM)

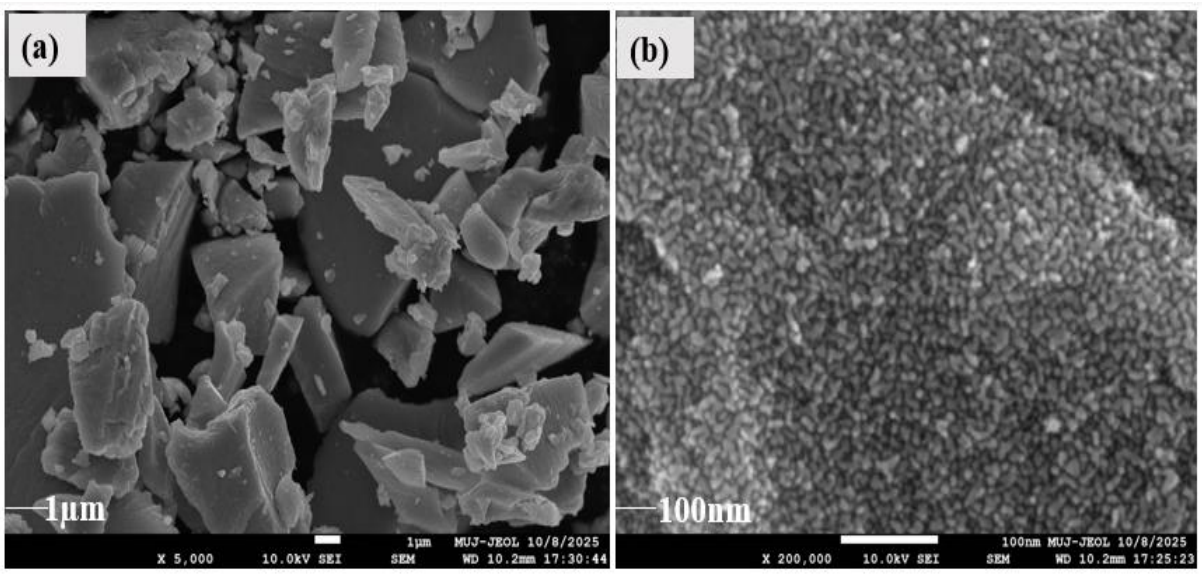

Fig. 3.8 FESEM of SnO_2 synthesized by the hydrothermal method at scales of (a) 1µm and (b) 100nm.

From the above figure, it was clearly observed that the hydrothermally synthesized SnO_2 have uniform and densely packed nanoparticles. At 1 µm, particle agglomeration was clearly observed. At the 100 nm scale, the particle appears nearly spherical and nanosized. The particle size was estimated to be approximately 16.57nm, which indicates agglomeration of nanoparticles.

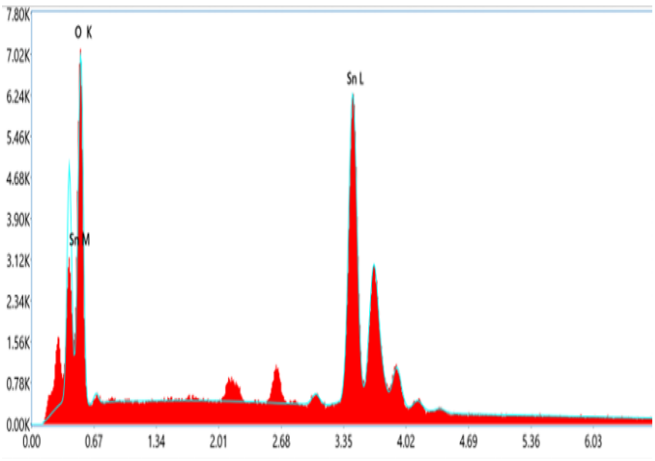

Fig. 3.9 EDX analysis of hydrothermally synthesized SnO_2

The elemental composition of SnO_2 synthesized by the hydrothermal method was studied using EDX (Energy Dispersive X-Ray analysis). This analysis confirmed the presence of Oxygen and Tin as the major elements of the nanomaterial without any impurities. The weight percentage of Oxygen was found to be 14.4% and 85.6% for tin, respectively. The atomic percentages were 55.5% for Oxygen and 44.5% for tin.

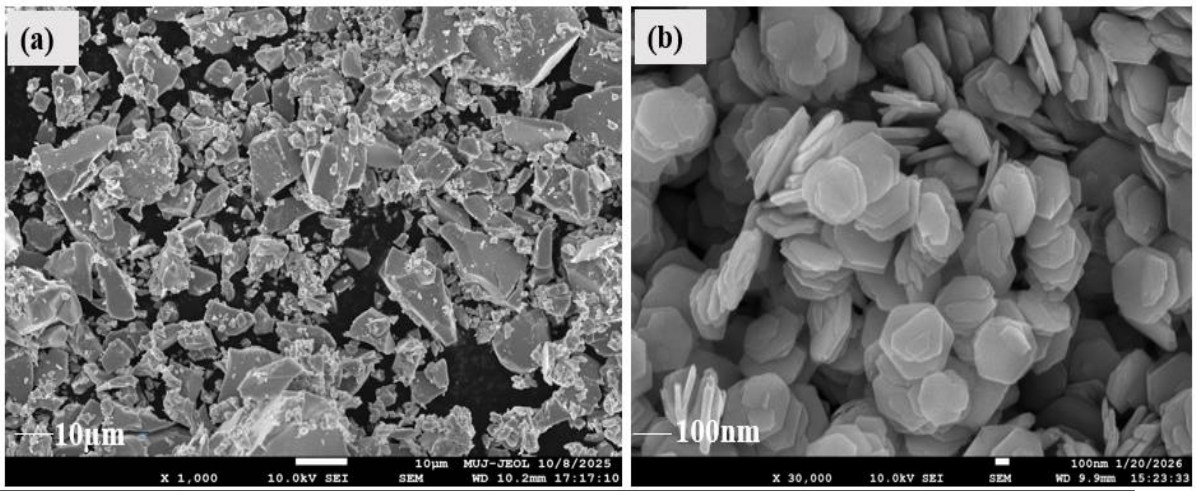

Fig. 3.10 FESEM of SnS_2 synthesized via (a) Co-precipitation and (b) Hydrothermal method.

Fig. 3.10 (a) reveals that particles are small and irregularly shaped with a particle size of 12 nm, while the hydrothermal sample Fig. 3.10 (b) showed a hexagonal thin plate morphology with a size of approximately 388nm.

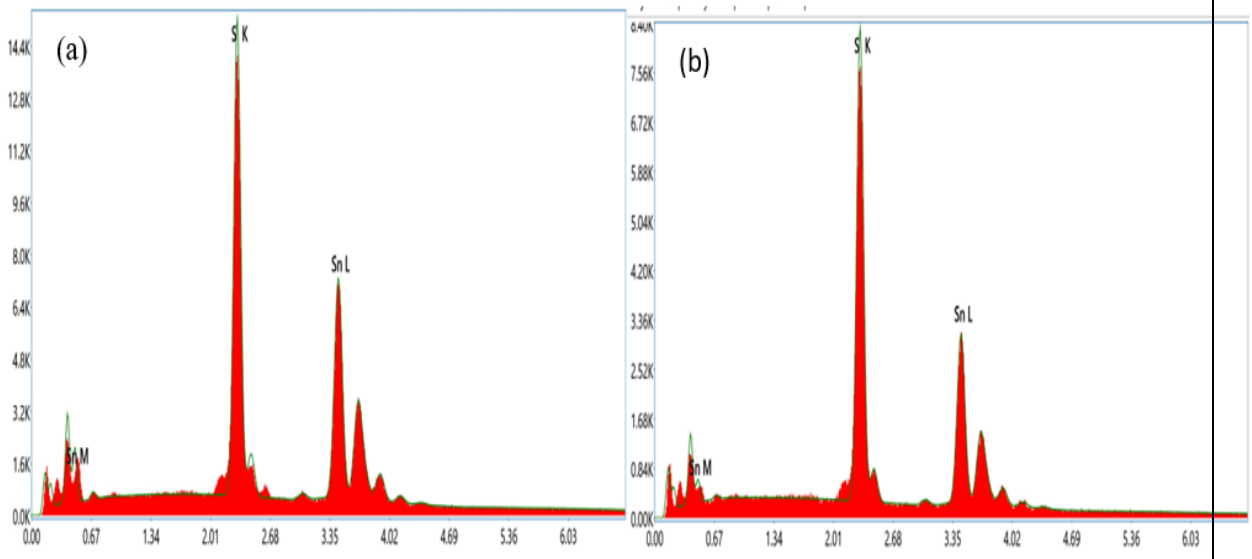

Fig. 3.11 EDX analysis of SnS_2 synthesized via (a) Co-precipitation and (b) Hydrothermal method

For the co-precipitation sample, the weight percentage of sulfur was found to be 26.1% and 73.9% for tin, respectively. The atomic percentages were 56.7% for sulfur and 43.3% for tin. While for the hydrothermal sample, the weight percentage of sulphur was found to be 31% and 69% for tin, respectively. The atomic percentages were 62.5% for sulfur and 37.5% for tin. This concludes that the hydrothermally synthesized SnS_2 results in better stoichiometric and compositional accuracy than the co-precipitation method.

3.2.3 Fourier Transform Infrared Spectroscopy

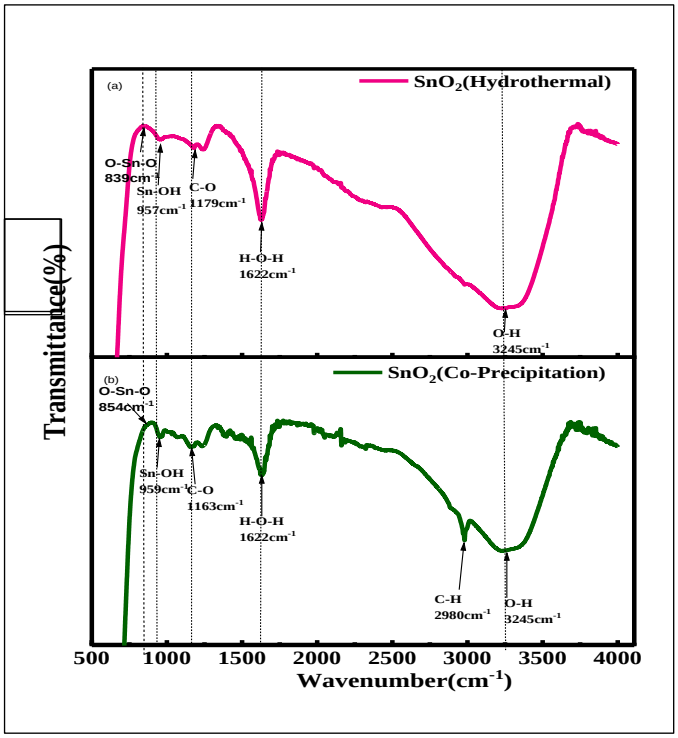

Fig. 3.12 FTIR of SnO_2 synthesized by the (a) Hydrothermal and (b) Co-precipitation method

FTIR spectroscopy was used to identify the functional groups present in the nanomaterial, and it was also used to confirm the formation of SnO_2 nanomaterials. For SnO_2 synthesized via the hydrothermal method, the significant peaks were observed at ~839 cm^{-1} and ~957 cm^{-1}, which are denoted to O-Sn-O and Sn-OH vibrations, which confirms the formation of tin oxide. A band at~1622 cm^{-1} corresponds to H-O-H bending, which indicates the presence of adsorbed water molecules [54]. The broad band at around ~3245 cm^{-1} is for O-H stretching vibrations, which belong to surface hydroxyl groups. Additionally, the C-O stretching at ~1179 cm^{-1} is due to residual organic species . For SnO_2 synthesized by the co-precipitation method, similar bonds and vibrations with slight peak shifts were observed. Peaks at ~859 cm^{-1} and ~959 cm^{-1} confirm Sn-O bonding, while the band at ~1632 cm^{-1} corresponds to adsorbed water. The presence of peaks around ~2980 cm^{-1} corresponds

to O-H bonding, which indicates more surface impurities or residual precursors when compared to the hydrothermal sample, suggesting relatively lower purity.

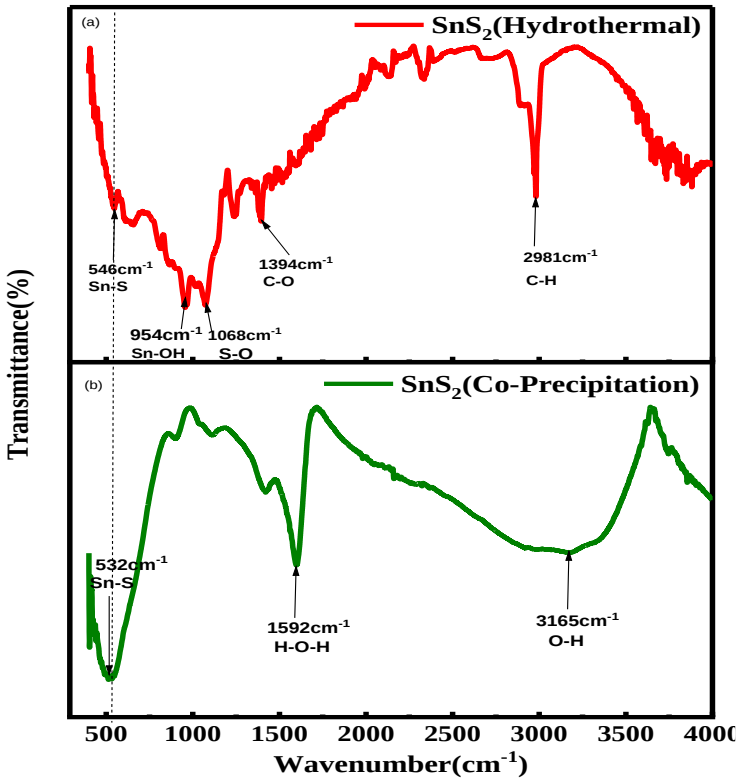

Fig. 3.13 FTIR of SnS_2 synthesized by the (a) Hydrothermal and (b) Co-precipitation method

FTIR spectroscopy was used to identify the functional groups present in the nanomaterial, and it was also used to confirm the formation of SnS_2 nanomaterials. In SnS_2 produced using the hydrothermal method, the peak around ~532 cm^{-1} is attributed to the Sn-S stretching vibration, which verifies the creation of tin disulfide. The bands around 954 cm^{-1} and 1068 cm^{-1} are associated with Sn-OH and S-O vibrations, suggesting surface oxidation and the adsorption of water molecules. The peak at ~1394 cm^{-1} is due to C-O stretching, while the band at ~2981 cm^{-1} is attributed to C-H vibrations, suggesting the presence of residual organic species [55]. In SnS_2 synthesized by the co-precipitation method, the Sn-S vibration appears at ~532 cm^{-1}, slightly shifted compared to the hydrothermal sample, which may be due to differences in crystallinity and particle size. The peak at ~1592 cm^{-1} corresponds to H-O-H

bonding, and the band at ~3165 cm^{-1} corresponds to O-H stretching vibrations [56]. This concludes that the co-precipitation sample has fewer impurity peaks when compared to the hydrothermal sample, which indicates cleaner surface chemistry.

3.2.4 UV-Visible Spectroscopy

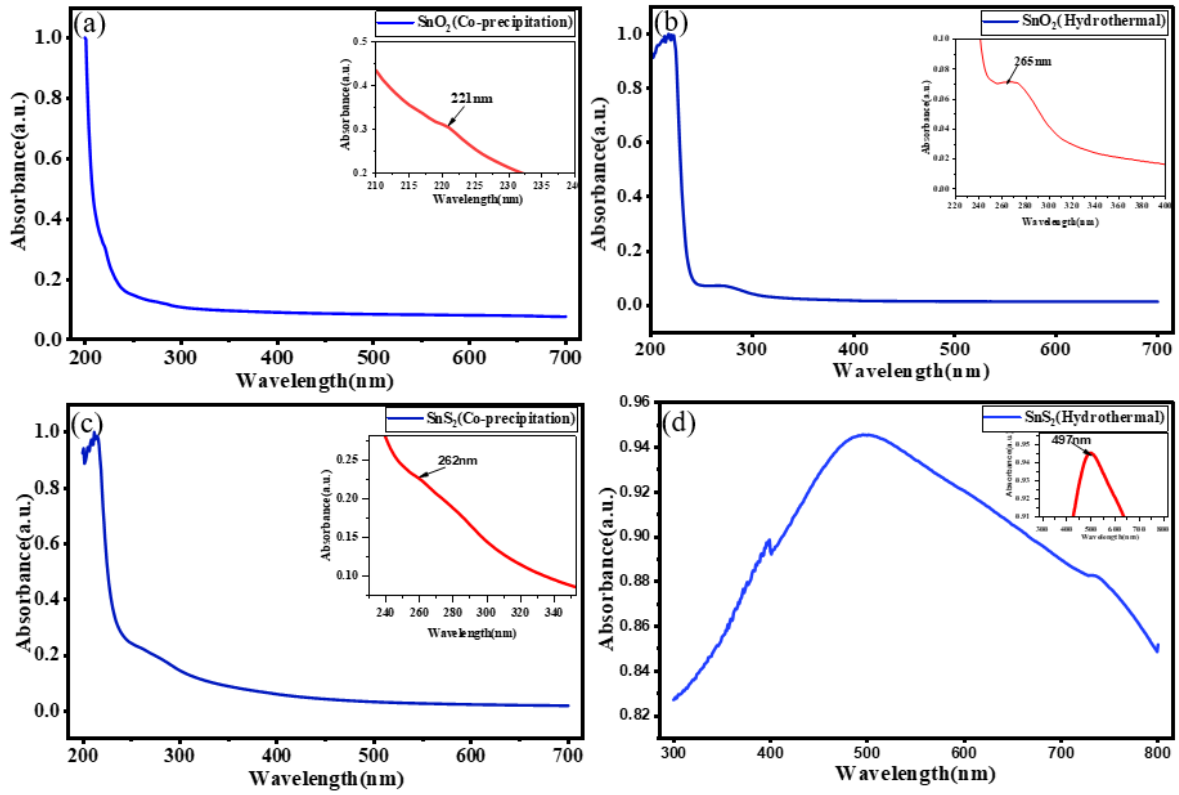

Fig. 3.14 UV-Vis spectra of (a) SnO_2 by co-precipitation method, (b) SnO_2 by hydrothermal method, (c) SnS_2 by co-precipitation method and (d) SnS_2 by hydrothermal method

The UV-Visible absorption spectra for SnO_2 and SnS_2 nanomaterials were recorded in the wavelength range of 200-800 nm. The UV region ranges from 200-400 nm, and the Visible region ranges from 400-800 nm [57]. The spectra are plotted as absorbance versus wavelength (as shown in Fig. 3.14), which represents the interaction of electromagnetic radiation with the material. For SnO_2, both samples exhibit strong absorption in the ultraviolet region; the hydrothermally synthesized sample fig. 3.14(b) shows relatively sharper and more intense absorption compared to the co-precipitation

sample fig. 3.14(a). This change may be due to its smaller crystallite size, which leads to enhanced interaction with incident radiation. SnO_2 prepared by the co-precipitation method exhibits peaks at 221nm, whereas SnO_2 prepared by the hydrothermal method exhibits peaks at 265nm. The co-precipitation sample of SnS_2, Fig. 3.14(c), exhibits high absorption in the UV spectrum range with reduced absorbance, while the hydrothermal sample, Fig. 3.14(d), has wide absorption in the visible spectrum range due to changes in optical properties because of varying synthesis techniques. SnS_2 synthesized by the co-precipitation method shows a peak at 262nm, whereas the hydrothermal sample shows a peak at 497nm [58]. This difference proves that the synthesis technique greatly affects the optical absorbance of SnO_2 and SnS_2.

CHAPTER-4

CONCLUSION, FUTURE SCOPE & SOCIAL IMPACT

4.1 CONCLUSION

In this work, SnO_2 and SnS_2 nanomaterials were successfully synthesized via co-precipitation and hydrothermal methods. XRD study confirmed the formation of crystalline phases, with variation in crystallite size depending on the synthesis route. The hydrothermal method produced a smaller crystallite size for SnO_2, while the co-precipitation method produced smaller crystallites for SnS_2. This shows that the growth mechanism depends a lot on the composition of the material. FTIR results confirmed the existence of distinctive bonding and functional groups, thereby validating the successful synthesis of SnO_2 and SnS_2 nanomaterials. The FESEM images showed that the SnO_2 made by hydrothermal synthesis has spherical particles that are very small. The SnS_2 made by the same method has a hexagonal thin plate morphology. The Co-precipitation method, on the other hand, made SnS_2 with smaller, more irregularly shaped particles. Studies of UV–Visible absorption showed that all samples absorbed a lot of UV light, except for hydrothermally synthesized SnS_2, which absorbed light in the visible spectrum. Overall, the results show that the synthesis method and material structure together influence the structural, morphological, and optical properties of the prepared nanomaterials.

4.2 FUTURE SCOPE

In this context, many avenues exist to explore further about SnO_2 and SnS_2 nanomaterials for various technological applications and scientific studies. In our further study on SnO_2 and SnS_2 nanomaterials, various parameters, including temperature, pH, reaction time, and precursor concentrations, could be adjusted in order to get fine control over particle size, morphology and crystallinity of the nanomaterials. It is possible to modify optical, electrical and catalytic properties of these nanomaterials by using other appropriate metal or non-metal dopants.

Characterization using TEM, PL spectroscopy, Raman spectroscopy and measurements of electrical conductivity could be carried out to have a better understanding of defects, charge transport properties and surface states of the synthesized nanomaterials. Moreover, the Photocatalytic properties and gas-sensing applications of these SnO_2 and SnS_2 nanomaterials need to be studied systematically for environmental applications and various industrial purposes. Under hydrothermal synthesis conditions, the SnO_2 and SnS_2 showed light absorption in the visible region. The study on these nanomaterials may focus on the applications for solar energy conversion, photodetectors and optoelectronic devices. It might be possible to synthesize thin films and nanocomposites using SnO_2 and SnS_2-based materials for their utilization as energy storage devices, sensors and in semiconductor technology.

4.3 SOCIAL IMPACT

The social and technological relevance of the synthesis and research of SnO_2 and SnS_2 nanomaterials stems from their possible use in the fields of environmental remediation, energy, and electronics. In environmental monitoring, gas sensors, and photocatalytic degradation processes involving these nanomaterials, they are expected to serve as effective devices in detecting and removing environmental pollutant species in water and air. SnS_2 is one material that shows the ability to absorb visible light, which is a positive attribute for solar energy devices. The development of such materials is expected to play an important role in the renewable energy sector in lessening the consumption of fossil fuels and also in reducing environmental pollution. The other SnO_2-based materials are broadly used in electronic devices, transparent conducting coatings, sensing technologies, and other fields, which are vital to current technology involving telecommunications, medical treatments, and industrial practices.

REFERENCES

[1] Alagarasi, A., 2013. Introduction to Nanomaterials. Chennai: Anna University.

[2] Findik, F., 2021. Nanomaterials and their applications. *Periodicals of Engineering and Natural Sciences*, 9(3), pp. 62–75.

[3] Kolahalam, L.A., Kasi Viswanath, I.V., Diwakar, B.S., Govindh, B., Reddy, V. and Murthy, Y.L., 2019. Review on nanomaterials: Synthesis and applications. *Materials Today: Proceedings*, 18, pp. 2182–2190.

[4] Badgayan, N.D., Sahu, S.K., Samanta, S. and Sreekanth, R.P.S., 2020. An insight into mechanical properties of polymer nanocomposites reinforced with multidimensional filler system: A state of art review. *Materials Today: Proceedings*, 24, pp. 422–431.

[5] Mazari, S.A., Ali, E., Abro, R., Ahmed Khan, F.S., Ahmed, I., Ahmed, M., Din, S., Siddiqui, T.H., Hossain, N., Mubarak, N.M. and Shah, A., 2021. Nanomaterials: Applications, waste-handling, environmental toxicities, and future challenges – A review. *Journal of Environmental Chemical Engineering,* 9, 105028.

[6] Chavali, M.S. and Nikolova, M.P., 2019. Metal oxide nanoparticles and their applications in nanotechnology. *SN Applied Sciences*, 1, pp. 1–30.

[7] Balakrishnan, A., Groenewold, J., Pokhrel, S. and Mädler, L., 2022. Metal sulfide nanoparticles: *Precursor chemistry. Chemistry – A European Journal*, 28(4).

[8] Das, S. and Jayaraman, V., 2014. SnO_2: A comprehensive review on structures and gas sensors. *Progress in Materials Science*, 66, pp. 112–255.

[9] Patil, G.E., Kajale, D.D., Gaikwad, V.B. and Jain, G.H., 2012. Preparation and characterization of SnO_2 nanoparticles by hydrothermal route. *International Nano Letters*, 2, pp. 1–7.

[10] Hwang, J.S., Kim, H.J., Lee, C.M. and Kim, Y.P., 2011. Paper-based disposable sensor fabricated via digital image analysis for trace determination of cyanide in water. *Microchemical Journal*, 98(2), pp. 256–260.

[11] Luo, L., Zhang, X., Wang, Y., Wang, Z., Yang, H. and Zhao, Y., 2019. Study of the bioavailability of heavy metals from atmospheric deposition on the soil–peach (Prunus persica L.) system. *Journal of Hazardous Materials*, 367, pp. 448–456.

[12] Cui, Y., Wang, L., Li, X., Zhao, X., Wang, Y. and Yang, T., 2018. Facile and ultrasensitive urea detection in fertilization process with cheap quantum dots and ion filter effect. Sensors and Actuators B: *Chemical*, 260, pp. 1043–1051.

[13] Kong, X., Yu, T., Zhang, L., Du, J., Tang, D., Wang, L. and Tao, Y., 2020. SnO_2 nanostructured materials used as gas sensors for the detection of hazardous and flammable gases: A review. *Nano Materials Science*, 2(1), pp. 1–13.

[14] Wu, C., Xu, X., Li, Y., Yu, Z., He, J. and Lin, J., 2020. Doping lithium element to enhance compressive strength of β-TCP scaffolds manufactured by 3D printing for bone tissue engineering. *Journal of Alloys and Compounds*, 820, 153153.

[15] Seri, M.A., Kawai, M. and Iwamoto, M., 2015. Thermodynamic analysis of glycerol steam reforming for hydrogen production with in situ hydrogen and carbon dioxide separation. *Journal of Power Sources*, 286, pp. 354–363.

[16] Zhao, D., Yu, Y., Wang, C., Lunt, R.R., Krylov, A.S., Ellingson, R.J. and Song, Y., 2017. Low-bandgap mixed tin-lead iodide perovskite absorbers with longer lifetimes for all-perovskite tandem solar cells. *Nature Energy*, 2, 17018.

[17] Nakato, T., Yamada, Y. and Kuroda, K., 1992. Mesophase of colloidally dispersed nanosheets prepared by exfoliation of layered titanate. *Journal of the Chemical Society, Chemical Communications*, (23), pp. 1739–1740.

[18] Iwasa, J., Takahashi, S., Asakura, Y. and Hosokawa, J., 2013. Influence of indium on carbon nanofibers based Cu/ZnO catalysts for liquid phase hydrogenation of CO_2 to methanol. *Catalysis Today*, 215, pp. 237–242.

[19]L.-y. Wang, H. Shen, Q. Yang, J. Min, Q. Wang, W. Xi, L. Yin, S.-g. Le, Y.-f. Zhang, J. Xiao, Z.-n. Wang, and G.-y. Ji, "LncRNA-LINC00472 contributes to the pathogenesis of atrial fibrillation (AF) by reducing expression of JP2 and RyR2 via miR-24*," Biochemical and Biophysical Research Communications,* vol. 120, Dec. 2019, Art. no. 109364.

[20] J. L. A. do Nascimento, L. Chantelle, I. M. G. dos Santos, A. L. M. de Oliveira, and M. C. F. Alves, "The influence of synthesis methods and experimental conditions on the photocatalytic properties of SnO2: *A review," Catalysts*, vol. 12, Art. no. 428, Apr. 2022.

[21] H. Wang and A. L. Rogach, "Hierarchical SnO2 nanostructures: Recent advances in design, synthesis, and applications," *Chemistry of Materials*, vol. 26, no. 1, pp. 123–133, 2014.

[22] Y. He, Y. Li, J. Yu, and Y. Qian, “Chemical control synthesis of nanocrystalline SnO2 by hydrothermal reaction,” *Materials Letters,* vol. 41, no. 1, pp. 23–26, 1999.

[23] Y. Huang, E. Sutter, J. T. Sadowski, M. Cotlet, O. L. A. Monti, D. A. Racke, M. R. Neupane, D. Wickramaratne, R. K. Lake, B. A. Parkinson, and P. Sutter, “Tin disulfide: An emerging layered metal dichalcogenide semiconductor: Materials properties and device characteristics,” *ACS Nano*, vol. 8, no. 10, pp. 10743–10755, 2014.

[24] J. M. Gonzalez and I. I. Oleynik, “Layer-dependent properties of SnS2 and SnSe2 two-dimensional materials,” *Physical Review B*, vol. 94, no. 12, Art. no. 125443, 2016.

[25] J. L. A. do Nascimento, L. Chantelle, I. M. G. dos Santos, A. L. M. de Oliveira, and M. C. F. Alves, “The influence of synthesis methods and experimental conditions on the photocatalytic properties of SnO2: *A review,” Catalyst*s, vol. 12, Art. no. 428, Apr. 2022.

[26] Y. H. Kwon, D.-H. Kim, H.-K. Kim, and J. Nah, “Phosphorus-doped zinc oxide p-n homojunction thin film for flexible piezoelectric nanogenerators,” *Nano Energy*, vol. 17, pp. 358–366, 2015.

[27] Z. Yang, X. Xu, X. Liang, C. Lei, Y. Wei, P. He, B. Lv, H. Ma, and Z. Lei, “MIL-53(Fe)-graphene nanocomposites: Efficient visible-light photocatalysts for the selective oxidation of alcohols,” *Applied Catalysis B: Environmental*, vol. 191, pp. 42–49, 2016.

[28] C.-T. Lin, K.-J. Chen, K.-C. Tseng, and L.-K. Chu, “Spatially and temporally-resolved tryptophan fluorescence thermometry for monitoring the photothermal processes of gold nanorod suspensions,” *Sensors and Actuators B: Chemical*, vol. 257, pp. 940–948, 2018.

[29] Q. An, F. Zhang, X. Yin, Q. Sun, M. Zhang, J. Zhang, W. Tang, and Z. Deng, “High-performance alloy model-based ternary small molecule solar cells,” *Nano Energy*, vol. 31, pp. 312–319, 2017.

[30] A. Zuin, T. Cousseau, A. Sinatora, S. H. Toma, K. Araki, and H. E. Toma, “Lipophilic magnetite nanoparticles coated with stearic acid: A potential agent for friction and wear reduction,” *Tribology International*, vol. 114, pp. 333–340, 2017.

[31] C. Bermúdez-Jiménez, M. G. Romney, S. A. Roa-Flores, G. Martínez-Castañón, and H. Bach, “Hydrogel-embedded gold nanorods activated by plasmonic photothermy with potent antimicrobial activity,” *Nanomedicine: Nanotechnology, Biology, and Medicine*, vol. 24, Art. no. 102093, 2020.

[32] S. H. Chaki, M. P. Deshpande, D. P. Trivedi, J. P. Tailor, M. D. Chaudhary, and K. Mahato, "Wet chemical synthesis and characterization of SnS2 nanoparticles," *Journal of Materials Science*, vol. 47, no. 10, pp. 4352–4359, 2012.

[33] H. Tian, C. Fan, G. Liu, Y. Zhang, M. Wang, and E. Li, "Hydrothermal synthesis and fast photoresponsive characterization of SnS2 hexagonal nanoflakes," *Journal of Materials Science*, vol. 54, no. 2, pp. 1617–1626, 2019.

[34] S. Gopal, S. Rajagemberam, B. Iruson, S. Balaraman, S. Krishnmoorthy, and M. Elayaperumal, "Study on structural, luminescence properties and Hall effect of SnO2 nanoparticles obtained by a co-precipitation technique*," International Journal of Nano Dimensions*, vol. 10, no. 3, pp. 242–251, 2019.

[35] M. A. M. Akhir, K. Mohamed, H.-L. Lee, and S. A. Rezan, "Synthesis of tin oxide nanostructures using hydrothermal method and optimization of its crystal size by using statistical design of experiment," *Procedia Chemistry*, vol. 19, pp. 993–998, 2016.

[36] S. Kota, A. S. Bharath, T. Dhayakaran, U. Munegowda, and B. K. Devendra, "Synthesis and characterization of SnS2 nanoparticles for enhanced photocatalytic and electrochemical sensing applications," *Tetrahedron Green Chemistry*, vol. 5, Art. no. 100067, 2025.

[37], [59] Wang, C., Tang, K., Yang, Q., Qian, Y., & Xu, C. (2001). Hydrothermal synthesis and characterization of SnS_2 nanocrystals. *Chemistry Letters*, 30(10), 998–999.

[38] Giannini, C., Ladisa, M., Altamura, D., Siliqi, D., Sibillano, T., & De Caro, L. (2016). X-ray diffraction: A powerful technique for the multiple-length-scale structural analysis of nanomaterials. *Crystals*, 6(8), 87.

[39] Bragg, W. H. (1929). Diffraction of X-rays by two-dimensional crystal lattice. *Nature*, 124, 125–126.

[40] Parczewski, K., & Wnek, H. (2018). Influence of car tire aspect ratio on driving through road unevenness. In Proceedings of the 22nd International Scientific Conference: Transport Means 2018 (pp. 321–325).

[41] Rohat, M.-C. (2012). Real-time rendering of translucent materials (Master's thesis, Technical University of Denmark). Informatics and Mathematical Modelling, IMM-MSc-2012-0060.

[42] Prabhu, R. S., Priyanka, R., Vijay, M., & Vikashini, G. R. K. (2021). Emission scanning electron microscopy (FESEM) with a very big future in pharmaceutical research. *International Journal of Pharmacy and Biological Sciences-IJPBS*, 11(2), 183–187.

[43] Slater, T. J. A., Janssen, A., Camargo, P. H. C., Burke, M. G., Zaluzec, N. J., & Haigh, S. J. (2015). STEM-EDX tomography of bimetallic nanoparticles: A methodological investigation. Ultramicroscopy, 162, 61–73.

[44] Cossu, C. (2021). Evaluation of tilt control for wind-turbine arrays in the atmospheric boundary layer. arXiv preprint arXiv:2009.13901.

[45] Shimadzu Corporation. Principles of FTIR spectroscopy and FTIR measurement techniques. Shimadzu Analytical and Measuring Instruments.

[46] Jurablu, S., Farahmandjou, M., & Pormirjaafari Firoozabadi, T. (2015). Multiple-layered structure of obelisk-shaped crystalline nano-ZnO prepared by sol–gel route. *Journal of Theoretical and Applied Physics*, 9, 261–266.

[47] Kumar, A., Meenakshi, Saxena, N., Seema, K., Srivastava, A., Rajak, J., Singh, D., Singh, S. V., & Singh, L. (2023). Physico-chemical characterization of green synthesized nanomaterials by UV-visible spectroscopy. *Current Nanomaterials*, 8(2), 102–118.

[48] Rathidevi, J., & Merlin H. (2018). Determination of lead in soil sample and validation on multiwall carbon nanotube modified electrode. *J. Nanosci. Tech*., 4(5), 564–566.

[49] Abdalkreem, T. M., Swart, H. C., & Kroon, R. E. (2023). Comparison of Y_2O_3 nanoparticles synthesized by precipitation, hydrothermal and microwave-assisted hydrothermal methods using urea. *Nano-Structures & Nano-Objects*, 35, 101026.

[50] Ohgi, H., Maeda, T., Fujihara, S., & Imai, H. (2004). Preparation of porous SnO_2 particles having high specific surface area and high thermal stability via an aqueous solution route and subsequent hydrothermal treatment. *Chemistry Letters*, 33(6), 706–707.

[51] N. V. Venkatesh, S. Aravindan, K. Ramki, G. Murugadoss, R. Thangamuthu, and P. Sakthivel, “Sunlight-driven enhanced photocatalytic activity of bandgap narrowing Sn-doped ZnO nanoparticles,” *Environmental Science and Pollution Research*, vol. 28, pp. 17659–17671, 2021.

[52] H. Uchiyama, Y. Shirai, and H. Kozuka, "Formation of spherical SnO_2 particles consisting of nanocrystals from aqueous solution of $SnCl_4$ containing citric acid via hydrothermal process," *Journal of Crystal Growth,* vol. 319, pp. 70–78, 2011.

[53] C. Fanelli, V. Cregan, F. Font, and T. G. Myers, "Nanocrystal growth via the precipitation method," arXiv preprint arXiv:1901.08990, 2019.

[54] A. H. Mahmood and E. J. Harjan, "On the dependent elements of reverse bimultipliers," *Iraqi Journal of Science,* vol. 57, no. 2, pp. 972–978, 2016.

[55] Y. Li, M. Zhou, G. I. N. Waterhouse, J. Sun, W. Shi, and S. Ai, "Efficient removal of cadmium ions from water by adsorption on a magnetic carbon aerogel*," Environmental Science and Pollution Research*, 2020.

[56] Preeti Kumari, Rimpal Morya, Hemant K. Arora, Sunil Kumar, Nikita Jain, Jasvir Dalal, and Nitin K. Puri, "Structural and optical properties of SnS_2 nanosheets for opto-electronic devices," Discover Materials, vol. 6, article 120, 2026.

[57] Z. Huang, J. Zhu, Y. Hu, Y. Zhu, G. Zhu, L. Hu, Y. Zi, and W. Huang, "Tin oxide (SnO_2) nanoparticles: Facile fabrication, characterization, and application in UV photodetectors," *Nanomaterials,* vol. 12, no. 4, article 632, 2022.

[58] C. I. Hussain, Y. M. Hassan, and F. A. Abed, "A comparative study of coprecipitation and solvothermal techniques for synthesizing pure and Cu-doped SnO_2 nanoparticles," *Nanomaterials and Nanotechnology*, vol. 2024, article ID 6155001, 2024.

24/phdap/14 BHARAT BHUSHAN

finalized thesis with refernces

NFL

Document Details

Submission ID
trn:oid:::27535:140686083

Submission Date
May 27, 2026, 11:05 PM GMT+5:30

Download Date
May 27, 2026, 11:09 PM GMT+5:30

File Name
finalized thesis with refernces.docx

File Size
3.5 MB

68 Pages

13,100 Words

77,262 Characters

turnitin Page 1 of 76 - Cover Page Submission ID trn:oid:::27535:140686083

10% Overall Similarity

The combined total of all matches, including overlapping sources, for each database.

Filtered from the Report

- Bibliography
- Quoted Text
- Cited Text
- Small Matches (less than 12 words)

Match Groups

71 Not Cited or Quoted 10%
Matches with neither in-text citation nor quotation marks

0 Missing Quotations 0%
Matches that are still very similar to source material

0 Missing Citation 0%
Matches that have quotation marks, but no in-text citation

0 Cited and Quoted 0%
Matches with in-text citation present, but no quotation marks

Top Sources

6% Internet sources
4% Publications
7% Submitted works (Student Papers)

Integrity Flags

0 Integrity Flags for Review

Our system's algorithms look deeply at a document for any inconsistencies that would set it apart from a normal submission. If we notice something strange, we flag it for you to review.

A Flag is not necessarily an indicator of a problem. However, we'd recommend you focus your attention there for further review.

turnitin Page 2 of 76 - Integrity Overview Submission ID trn:oid::27535:140686083

Match Groups

- 71 Not Cited or Quoted 10%
  Matches with neither in-text citation nor quotation marks
- 0 Missing Quotations 0%
  Matches that are still very similar to source material
- 0 Missing Citation 0%
  Matches that have quotation marks, but no in-text citation
- 0 Cited and Quoted 0%
  Matches with in-text citation present, but no quotation marks

Top Sources

6% Internet sources
4% Publications
7% Submitted works (Student Papers)

Top Sources

The sources with the highest number of matches within the submission. Overlapping sources will not be displayed.

1	Student papers	
	Delhi Technological University on 2026-05-20	<1%
2	Student papers	
	Delhi Technological University on 2026-05-07	<1%
3	Publication	
	Sumanjali Kota, Akshay Shivashankar, Tushvitha Dhayakaran, Uthkruthi Munego...	<1%
4	Internet	
	www.ijnd.ir	<1%
5	Publication	
	C. Pandurangappa, B.N. Lakshminarasappa, B.M. Nagabhushana. "Synthesis and ...	<1%
6	Student papers	
	Delhi Technological University on 2026-04-29	<1%
7	Student papers	
	Delhi Technological University on 2026-04-09	<1%
8	Student papers	
	National Institute of Technology Delhi on 2026-05-21	<1%
9	Student papers	
	Higher Education Commission Pakistan on 2016-08-16	<1%
10	Publication	
	Akhir, Maisara A.M., Khairudin Mohamed, H.L. Lee, and Sheikh A. Rezan. "Synthes...	<1%

turnitin Page 3 of 76 - Integrity Overview Submission ID trn:oid:::27535:140686083

11	Student papers	
Delhi Technological University on 2026-05-25		<1%
12	Student papers	
Loughborough University on 2016-01-08		<1%
13	Internet	
archive.org		<1%
14	Internet	
storage.freidok.ub.uni-freiburg.de		<1%
15	Student papers	
IIT Delhi on 2014-04-24		<1%
16	Internet	
repository.iutoic-dhaka.edu		<1%
17	Internet	
c.coek.info		<1%
18	Student papers	
Waterford Institute of Technology on 2018-02-19		<1%
19	Student papers	
Federal University of Technology on 2025-01-16		<1%
20	Student papers	
Higher Education Commission Pakistan on 2013-07-02		<1%
21	Student papers	
National University of Singapore on 2012-04-10		<1%
22	Student papers	
Coventry University on 2008-02-22		<1%
23	Publication	
Devendra Patel, Shyama Prasad Mahapatra. "Synthesis, characterizations, dielect...		<1%
24	Student papers	
University College London on 2023-01-31		<1%

25 Internet
dspace.iiti.ac.in <1%

26 Internet
link.springer.com <1%

27 Student papers
Guru Ghasidas Vishwavidyalaya, Bilaspur on 2026-05-14 <1%

28 Student papers
Higher Education Commission Pakistan on 2012-06-07 <1%

29 Student papers
Savitribai Phule Pune University on 2015-07-01 <1%

30 Internet
ethesis.nitrkl.ac.in <1%

31 Internet
research.library.mun.ca <1%

32 Publication
Arik Kar, Simanta Kundu, Amitava Patra. " Surface Defect-Related Luminescence ... <1%

33 Publication
Dave, Hareshkumar Kantilal. "Studies on the Performance of Pervaporation for th... <1%

34 Student papers
Delhi Technological University on 2026-05-07 <1%

35 Student papers
Higher Education Commission Pakistan on 2025-06-23 <1%

36 Student papers
University of Witwatersrand on 2025-07-02 <1%

37 Student papers
Visvesvaraya Technological University on 2014-11-15 <1%

38 Internet
repository.um-palembang.ac.id <1%

39	Internet	
scholar.uoc.ac.in		<1%
40	Internet	
www.thenanoresearch.com		<1%
41	Publication	
Beibei Zhang, Guojun Dong, Lei Wang, Yajun Zhang, Yong Ding, Yingpu Bi. " Effici...		<1%
42	Student papers	
Delhi Technological University on 2026-04-21		<1%
43	Publication	
Dilip L. Kamble, Namdev S. Harale, Vithoba L. Patil, Pramod S. Patil, Laxman D. Ka...		<1%
44	Student papers	
Indian Institute of Technology Jodhpur on 2021-05-25		<1%
45	Student papers	
Savitribai Phule Pune University on 2017-12-07		<1%
46	Student papers	
University of Dundee on 2026-04-17		<1%
47	Student papers	
University of Malaya on 2013-06-15		<1%
48	Student papers	
University of Sheffield on 2024-02-08		<1%
49	Internet	
catalysis.blog		<1%
50	Internet	
dspace.ncl.res.in:8080		<1%
51	Internet	
nanoscalereslett.springeropen.com		<1%
52	Internet	
rosdok.uni-rostock.de		<1%

53 Internet
www.researchgate.net <1%

54 Publication
Bawoke Mekuye, Rainer Höfer, Birhanu Abera. "Nanomaterials: Terms, Definition... <1%

55 Student papers
Global Banking Training on 2026-05-15 <1%

56 Student papers
Gomal University on 2026-02-04 <1%

57 Student papers
Griffith College Dublin on 2024-04-09 <1%

58 Publication
Kai Zhu, Dandan Tang, Kaicheng Zhang, Zhaowei Wang, Lan Ding, Yanfeng Liu, Li... <1%

59 Publication
Rajwali Khan, Fazal Raziq, Iftikhar Ahmad, Kashif Safeen et al. "Advances in fabric... <1%

60 Student papers
University of Leicester on 2026-05-27 <1%

61 Student papers
University of Limerick on 2024-11-11 <1%

62 Student papers
University of Reading on 2026-05-21 <1%

63 Student papers
University of South Africa on 2026-05-27 <1%

64 Publication
Yulin Kong, Yuxiu Li, Xiuxiu Cui, Linfeng Su, Dian Ma, Tingrun Lai, Lijia Yao, Xuech... <1%

65 Internet
ruor.uottawa.ca <1%

66 Internet
v.vibdoc.com <1%

67 Internet
www.coursehero.com <1%

*% detected as AI

AI detection includes the possibility of false positives. Although some text in this submission is likely AI generated, scores below the 20% threshold are not surfaced because they have a higher likelihood of false positives.

Caution: Review required.

It is essential to understand the limitations of AI detection before making decisions about a student's work. We encourage you to learn more about Turnitin's AI detection capabilities before using the tool.

Disclaimer

Our AI writing assessment is designed to help educators identify text that might be prepared by a generative AI tool. Our AI writing assessment may not always be accurate (i.e., our AI models may produce either false positive results or false negative results), so it should not be used as the sole basis for adverse actions against a student. It takes further scrutiny and human judgment in conjunction with an organization's application of its specific academic policies to determine whether any academic misconduct has occurred.